Dual Functions of SPOP and ERG Dictate Androgen Therapy Responses in Prostate Cancer

Tiziano Bernasocchi[1,2*], Geniver El Tekle[1,2*], Marco Bolis[1*], Azzurra Mutti[1], Arianna Vallerga[1], Laura P. Brandt[3], Filippo Spriano[1,2], Tanya Svinkina[4], Marita Zoma[1,2], Valentina Ceserani[1], Anna Rinaldi[1], Hana Janouskova[1], Daniela Bossi[1], Manuela Cavalli[1], Simone Mosole[1], Roger Geiger[5], Ze Dong[6], Cai-Guang Yang[6], Domenico Albino[1], Andrea Rinaldi[1], Peter Schraml[7], Simon Linder[8], Giuseppina M. Carbone[1], Andrea Alimonti[1], Francesco Bertoni[1], Holger Moch[7], Steven A. Carr[4], Wilbert Zwart[8], Marianna Kruithof-de Julio[3], Mark A. Rubin[3], Namrata D. Udeshi[4], Jean-Philippe P. Theurillat[1+]

[*] These authors contributed equally to this work.

[+]Correspondence to: JeanP_Theurillat@ior.iosi.ch

[1]Institute of Oncology Research, Faculty of Biomedical Sciences, USI, Bellinzona, TI 6500, Switzerland. [2]University of Lausanne, Lausanne, VD 1011, Switzerland. [3]Department of Biomedical Research, University of Bern, 3008 Bern, Switzerland. [4]The Broad Institute of MIT & Harvard, Cambridge, MA 02142, USA. [5]Institute for Research in Biomedicine, Bellinzona, TI 6500, Switzerland. [6]State Key Laboratory of Drug Research, Shanghai Institute of Materia Medica, Chinese Academy of Sciences, Shanghai 201203, China. [7]Department of Pathology and Molecular Pathology, University Hospital Zurich, Zurich, ZH 8091, Switzerland. [8]The Netherlands Cancer Institute, Oncode Institute, 1066CX Amsterdam, Netherlands.

Driver genes with a mutually exclusive mutation pattern across tumor genomes are thought to have overlapping roles in tumorigenesis. In contrast, we show here that mutually-exclusive prostate cancer driver alterations involving the *ERG* transcription factor and the ubiquitin ligase adaptor *SPOP* are synthetic sick. At the molecular level, the incompatible cancer pathways are driven by opposing functions in SPOP. ERG up-regulates wild type SPOP to dampen androgen receptor (AR) signaling and sustain ERG activity through degradation of the bromodomain histone reader ZMYND11. Conversely, SPOP-mutant tumors stabilize ZMYND11 to repress ERG-function and enable oncogenic androgen receptor signaling. This dichotomy regulates the response to therapeutic interventions in the AR pathway. While mutant SPOP renders tumor cells susceptible to androgen deprivation therapies, ERG promotes sensitivity to high-dose androgen therapy and pharmacological inhibition of wild type SPOP. More generally, these results define a distinct class of antagonistic cancer drivers and a blueprint toward their therapeutic exploitation.

Normal cells transform into cancer cells by the acquisition of genetic aberrations in so called driver genes. In some instances, the functional redundancy of mutations in different genes result in a mutually-exclusive mutation pattern across tumor genomes because one alteration is sufficient to activate the specific oncogenic pathway. Based on this assumption, bioinformatic tools have been generated to search for functional redundancy of mutated genes in larger cancer genome data sets[1,2].

In prostate cancer, recurrent gene fusions involving the *ERG* transcription factor and point mutations in the ubiquitin ligase adaptor *SPOP* are two truncal mutations that are mutually exclusively distributed across tumor genomes (Fig. 1a and Extended Data Fig. 1a)[3-7]. The underlying cause for this exquisite pattern remains controversial. While earlier reports suggested a functional redundancy between mutant SPOP and ERG based on the

49 finding that mutant SPOP stabilizes the ERG oncoprotein[8,9], more recent studies challenge
50 this view by showing descriptive evidence for divergence in tumorigenesis[3,10].
51
52 **RESULTS**
53 **Activation of the ERG oncogene and missense mutation in SPOP are synthetic sick**
54 To shed light into the functional relationship of these recurrent driver genes, we
55 assessed the impact of SPOP mutations and ERG activation on the cellular growth of
56 mouse prostate epithelial organoids. In agreement with recent reports, lentiviral-transduced
57 point mutants of SPOP (SPOP-Y87C, SPOP-W131G) or a truncated version of ERG,
58 which typically results from gene fusion with androgen-regulated genes in prostate cancer
59 (ΔERG, amino acids 33-486), promoted cell growth (Fig. 1b, Extended Data Fig. 1b)[11-14].
60 While SPOP mutant organoids displayed a round shape, the over-expression of ΔERG gave
61 rise to characteristic finger-like protrusions. Surprisingly, the joint expression of both
62 drivers considerably diminished cell growth and reduced finger-like protrusions, implying
63 a synthetic sick relationship between the two genetic alterations. Cytological follow up
64 analysis revealed reduced proliferation associated with senescence (evidenced by reduced
65 Ki-67, increased p16 and P-HP1y positivity) rather than cell death as underlying cause
66 (Extended Data Fig. 1c).
67 We wondered if the observed synthetic sick relationship also applied to established
68 cancer cells from advanced, castration-resistant metastatic disease. Forced expression of
69 mutant SPOP (SPOP-Y87C, SPOP-W131G) promoted 3D growth of *ERG* fusion-negative
70 LAPC-4 human prostate cancer cells. The oncogenic effect was paralleled by an increase
71 in the expression of the oncogenic transcription factors MYC and HOXB13 and a decrease

72 in the cell cycle inhibitor p21 as seen also in an organoid line derived from *Spop*^{F133V}-
73 mutant transgenic mice (Extended Data Fig. 1d, e)[11]. In contrast, we observed the opposite
74 phenotypic and molecular changes in VCaP human prostate cancer cells harboring the
75 recurrent *TMPRSS2-ERG* fusion (Fig. 1c, d & Extended Data Fig. 1f-h). In this setting,
76 mutant SPOP (SPOP-Y87C, -F102C, -W131G, -F133S) dramatically decreased the
77 proliferation of cancer cells in culture and the growth of xenograft tumor models *in vivo*.
78 Similarly, to the mouse prostate organoids, induction of senescence was evidenced by
79 upregulation of p21 and GDF15 protein levels. In line with this, the transfer of conditioned
80 medium from VCaP cells expressing mutant SPOP (SPOP-Y87C , SPOP-W131G)
81 reduced also the proliferation of parental VCaP cells, indicating a contribution of
82 Senescence-Associated Secretory Phenotype (SASP) to the synthetic sick relationship (Fig.
83 1d and Extended Data Fig. 1i).

84 Conversely, forced expression of ΔERG significantly reduced the growth of SPOP-
85 Y83C mutant LuCaP-147 patient-derived xenograft (PDX) cancer cells *in vivo* and in
86 culture (Fig. 1e, Extended Data Fig. 2a, b)[15], adding orthogonal support for a synthetic sick
87 relationship between mutant SPOP and ΔERG in advanced prostate cancer. In addition,
88 over-expression of MYC promoted cancer cell growth in both VCaP and LuCaP-147 cells
89 (Extended Data Fig. 2c, d). The latter finding largely excludes that the over-expression
90 system *per se* is the underlying cause of the synthetic sick relationship mentioned above.

91 Next, we wondered if genetic or pharmacologic suppression of ERG signaling may
92 revert the growth suppressing function of mutant SPOP in VCaP cells. Indeed, knockdown
93 of ERG by short-hairpin RNA interference decreased the growth of VCaP control cells and
94 of cells over-expressing wild-type SPOP, while it promoted the growth of cells over-

95 expressing SPOP-W131G (Extended Data Fig. 2e). In addition, low doses of the ETS
96 inhibitor YK-4-279 promoted specifically the growth of VCaP cells over-expressing
97 mutant SPOP (Fig. 1f). We noted a similar effect when VCaP cells were co-treated with a
98 small molecule inhibitor of SPOP (Extended Data Fig. 2f)[16]. In aggregate, the data support
99 an antagonistic relationship between oncogenic activation of ERG and a loss of SPOP
100 function in prostate cancer cells.
101

102 **Mutant SPOP induced androgen receptor signaling antagonizes ERG activity**

103 To assess the underlying molecular biology of the antagonistic relationship between
104 *ERG*-fused and *SPOP*-mutants tumors, we interrogated the transcriptomes from the TCGA
105 cohort to nominate differences across these tumor subtypes. Indeed, the unbiased principal
106 component analysis (PCA) revealed major differences in the transcriptional output
107 (Extended Data Fig. 2g). The differences were maintained in castration-resistant prostate
108 cancers (CRPC) from the (SU2C) cohort using a single-sample gene-set enrichment
109 analysis approach (Extended Data Fig. 2h). Furthermore, derived (PDX) models also
110 retained analogue transcriptional differences, as demonstrated by different behavior shown
111 by *SPOP*-Mutant (LuCaP-78, -147) and *ERG*-Fused (LuCaP-35, -23.1, VCaP cells) models
112 (Extended Data Fig. 2h).

113 In *SPOP*-mutant prostate cancer, several dysregulated SPOP substrates (e.g. NCOA3,
114 TRIM24, BET proteins) have been shown to boost the AR pathway leading ultimately to
115 high levels of AR target genes (Extended Data Fig. 2i)[3,11,17-24]. In contrast, *ERG*-fused
116 cancer cells express typically lower levels of AR target genes as illustrated by the widely
117 adopted AR score (Extended Data Fig. 2i)[3]. To get more insights into this different

118 behavior, we further performed differential expression analysis between the two tumor
119 subtypes. Gene-set enrichment analysis resulted in a clear up regulation of the canonical
120 androgen response pathway in *SPOP*-mutant versus *ERG*-fused tumors, as defined by the
121 respective Hallmark gene-set, curated by the Molecular Signature Database (MSigDB)
122 (Extended Data Fig. 2j). In line with the divergence of transcriptome profile identified in
123 the PCA plot of Extended Data Fig. 2g, a clear division between *SPOP*-mutant and *ERG*-
124 fused tumors was also reported in their respective cistrome counterpart[25]. By re-analyzing
125 ChIP-Seq data, we could determine that most differentially bound regions between both
126 tumor types, are indeed characterized by increased AR-binding in *SPOP*-mutant tumors
127 (Extended Data Fig. 2k).

128 Next, we analyzed the transcriptome changes of the VCaP cells overexpressing SPOP
129 mutants (SPOP-MTs; SPOP-Y87C, -F102C, -F133S). The unbiased hallmark analysis
130 showed a dramatic increase in the androgen response, recapitulating the changes identified
131 in primary prostate cancer (Extended Data Fig. 2j, 3a and 3b). Based on these results, we
132 posited that differential levels of androgen receptor (AR) signaling in *SPOP*-mutant versus
133 *ERG*-fused cancers might be at the root of the incompatibility between the driver events.
134 Thus, we analyzed in particular AR- and ERG-related transcription in VCaP cells, and
135 generated a custom signatures using ChIP-seq data and matched RNA-seq samples
136 (Supplementary Table 1)[25]. As expected, SPOP-MTs increased the transcription of genes
137 bound by AR and induced by its ligand dihydrotestosterone (DHT), whereas genes bound
138 by AR and repressed by DHT were further reduced (Fig. 2a, Extended Data Fig. 3c, and
139 Supplementary Data Table 1). Remarkably, we observed the opposite effect on genes
140 bound only by ERG. Mutant SPOP downregulated ERG-induced genes (e.g. MYC) and

141 upregulated ERG-repressed genes, respectively (Fig. 1d). In line with these findings, gene
142 ontology analysis of AR-ERG co-bound gene signature in VCaP cells indicated that the
143 most striking transcriptional changes were linked to cellular differentiation and cell cycle
144 arrest that are directly induced by DHT and repressed by ERG (e.g. HOXA genes,
145 CDKN1A/p21, Fig. 1d, Fig. 2b, Extended Data Fig. 3d). To reduce the number of genes
146 falling within our custom signatures, we used a particularly restrictive approach and
147 considered as co-bound only genes where AR and ERG binding sites were overlapping for
148 at least 1bp. As a result, some genes (i.e. CDKN1A/p21) which are bound both by AR and
149 ERG in their promoter region, but which bindings do not overlap, are not included in this
150 category despite being bona fide co-bound targets.

151 The dramatic upregulation of this gene set was paralleled by a downregulation of cell
152 cycle genes (e.g. E2F and MYC targets), implying a direct link between the induction
153 AR/ERG co-bound genes, the repression of ERG targets, cell differentiation and the
154 synthetic sick relationship of ERG and mutant SPOP (Fig. 1d, Extended Data Fig. 3a-e).
155 The relationship of AR- and ERG-related custom signatures to the hallmark gene sets are
156 highlighted in Fig. 2c in a two-dimensional network. Moreover, independently generated
157 signatures of senescence-associated transcripts were enriched in VCaP overexpressing
158 SPOP mutants, further corroborating our data of a senescence-induced cell cycle arrest (
159 Extended Data Fig. 3f)[26,27].

160 Conversely, we assessed the consequence of ERG over-expression in LNCaP cells
161 under low DHT levels where mutant SPOP triggers AR signaling and tumor growth
162 (Extended Data Fig. 3g,h)[17,21]. Over-expression of ΔERG in this setting robustly reverted
163 the induction of signatures related to cell proliferation (e.g. E2F and MYC targets) and AR

signaling. Taken together, the data implies a reciprocal incompatibility of mutant SPOP induced AR signaling and the function of the ERG oncogene.

Next, we verified if corresponding transcriptional changes were found in clinical tissue samples. Indeed, ERG-regulated genes culled from VCaP cells were up-regulated in *ERG*-fused and down-regulated in *SPOP*-mutant primary tumors (Fig. 2d, Extended Data Fig. 4a)[3]. Importantly, the most striking changes between the two groups were found again in the AR/ERG co-bound gene set in primary prostate cancers (Extended Data Fig. 4b)[3,6]. The results underscore both the relevance of our cell culture-based data and highlight the transcriptional differences among *ERG*- and *SPOP*-driven tumors.

ZMYND11 is a SPOP substrate that induces AR and represses ERG transcription

Using tandem mass tag (TMT)-based quantitative mass-spectrometry, we set out to search for SPOP substrates that may influence the activity of AR and ERG and thereby may cause to the synthetic sick relationship between mutant SPOP and ERG in VCaP cells overexpressing mutant SPOP (SPOP-MTs; SPOP-Y87C, -F102C, -W131G, Extended Data Fig. 4c). Because recurrent loss-of-function SPOP mutants impair substrate ubiquitylation and proteasomal degradation, we searched for proteins which expression levels increase without concomitant increase in mRNA levels (Fig. 3a, Extended Data Fig. 4c, d). Overall, we noted a strong correlation of protein with mRNA expression changes with consistent changes of our AR and ERG custom signatures at the protein level (Fig. 3a., Extended Data Fig. 4e). In addition, we found a marked upregulation of the known SPOP substrate and AR activator TRIM24 at the protein level (Fig. 1c & 3a, Supplementary Table 2)[20,21] and subsequently assessed if TRIM24 and more generally AR

187 is implicated in the synthetic sick relationship between mutant SPOP and ERG. Indeed,
188 knockdown of TRIM24 by two short hairpin RNAs partially reverted the growth inhibition
189 mediated by mutant-SPOP in VCaP cells and reduced AR signaling (Extended Data Fig.
190 4f, g), while over-expression of AR was sufficient to decrease cellular growth (Extended
191 Data Fig. 4h, i).

192 The most striking upregulation was noted for the bromodomain histone reader
193 ZMYND11 (Fig. 3a, Extended Data Fig. 4d). In line with a SPOP substrate, wild type
194 SPOP bound, ubiquitylated and decreased the expression of HA-ZYMND11 in a
195 proteasome-dependent manner (Extended Data Fig. 5a, b). We found two degron
196 sequences that were required for efficient SPOP-mediated ubiquitylation and protein
197 degradation (Extended Data Fig. 5c-f). As expected, SPOP mutants failed to bind and
198 adequately ubiquitylate HA-ZMNYD11-WT (Extended Data Fig. 5g-i)[8,9,18-20,22-24]. Finally,
199 we confirmed that expression of mutant SPOP prolonged the half-life of endogenous
200 ZMYND11 in VCaP cells and upregulated ZMYND11 expression in other prostate cancer
201 cells (Extended Data Fig. 5j, k).

202 Next, we assessed if ZMYND11 protein upregulation also contributed to the synthetic
203 sick relationship. In support, forced expression of the degron-deficient variants of
204 ZMYND11 (HA-ZMYND11-DMT1/DMT2) was sufficient to diminish the growth of
205 VCaP cells (Fig. 3b, Extended Data Fig. 6a, b), while knockdown of ZMYND11 partially
206 reverted the growth inhibition mediated by mutant SPOP (Fig. 3c).

207 We postulated that ZMYND11 up-regulation could contribute to the synthetic sick
208 relationship by repressing the transcriptional activity of the ERG oncogene or enhancing
209 AR signaling. To this end, expression changes induced by HA-ZMYND11-DMT2 largely

210 overlapped with genes perturbed by mutant SPOP while the opposite was noted when
211 ZMYND11 expression was reduced by RNA interference (Fig. 3c, d, Extended Data Fig.
212 6c). In comparison to mutant SPOP, AR and ERG target genes were similarly dysregulated
213 by HA-ZMYND11-DMT2 (Fig. 3e). Because the PWWP domain of ZMYND11 has been
214 involved in the regulation of transcription through its ability to bind H3K36me3 histone
215 marks[28], we tested the contribution of this domain to the overall transcriptional output.
216 Indeed, the PCA of VCaP cells over-expressing either HA-ZMYND11-DMT2 or a PWWP
217 domain deficient mutant (W294A) revealed a major contribution of this domain to the
218 ZMYND11 induced transcriptional changes (Extended Data Fig. 6d). We subsequently
219 mapped the genomic occupancy of ZMYND11 in VCaP cells expressing the SPOP-Y87C
220 mutant by chromatin immunoprecipitation sequencing (ChIP-seq) and found an
221 enrichment of ZMYND11 binding sites at promoter regions controlling ERG-induced
222 genes (e.g. MYC,) and AR/ERG co-bound genes (e.g. p21/CDKN1A) (Fig. 3b, f, g,
223 Extended Data Fig. 6e-i). The data imply a critical enhancer function of ZMYND11 in
224 boosting AR signaling and repressing ERG signaling downstream of mutant SPOP.
225

226 **Wild type SPOP is required for ERG oncogenic function**

227 We reasoned that ERG-driven tumors may require wild type SPOP to degrade
228 ZMYND11 and thereby unlock the oncogenic function of ERG. In support, over-
229 expression of wild type SPOP increased the 3D growth of mouse prostate epithelial
230 organoids and VCaP cells only when ERG was over-expressed (Fig. 1b, Extended Data
231 Fig. 2e, 7a, b). Remarkably, ERG-fused human tumor tissues displayed also the highest
232 SPOP mRNAs levels (Fig. 4a). Thus, we wondered if ERG itself may directly upregulate

233 SPOP transcription to support its own oncogenic activity. Indeed, mining ERG ChIP-seq
234 data in VCaP cells revealed ERG bindings sites in the promoter region of SPOP (Extended
235 Data Fig. 7c). Moreover, knockdown of ERG reduced SPOP protein levels in VCaP cells,
236 while forced expression of a ΔERG led to the upregulation of SPOP mRNA and protein
237 levels in PC3 cells (Fig. 4b, Extended Data Fig. 2e, 7d).

238 We then asked if the elevated SPOP levels in the context of forced ΔERG expression
239 have a functional impact on the oncogenic activity of ΔERG in the androgen-independent
240 PC3 cells, in which ERG promotes tumor cell invasion[29]. Indeed, the reduction of SPOP
241 levels by RNA interference reduced the ability of ΔERG to invade into matrigel (Fig. 4c).
242 Similarly, knockdown of SPOP in VCaP cells reduced cell growth in 3D cell culture and
243 impaired ERG-mediated gene transcription (Extended Data Fig. 7e, f). In accordance with
244 the ability of mutant SPOP to repress the function of endogenous wild type SPOP in a
245 dominant-negative manner, the over-expression of mutant SPOP (SPOP-Y87C, -F102C, -
246 W131G, -F133S) phenocopied the effect of SPOP knockdown on ERG-mediated invasion
247 in PC3 cells (Extended Data Fig. 7g, h). In agreement with the established repressive
248 function of ZMYND11 on ERG, we found that over-expression of HA-ZMNYD11-DM2
249 was sufficient to repress ERG-induced invasion and established target genes in PC3 cells
250 (Fig. 4d, e). Taken together, the data imply the existence of a positive feed-forward loop,
251 in which ΔERG promotes the expression of SPOP to sustain its oncogenic activity.

252

253 **ERG and mutant SPOP trigger different responses to therapeutic interventions**

254 Based on the above-mentioned differences in tumorigenesis, we speculated that ERG
255 or mutant SPOP could also trigger different therapeutic responses. In light of the

256 dependency of ERG-driven tumors on wild type SPOP function, we hypothesized that
257 *ERG*-fusion positive cells may be particularly sensitive to pharmacological inhibition of
258 SPOP. We analyzed the response of the SPOP small molecule inhibitor compound 6b
259 (SPOP-i) in *ERG*-fused, *SPOP* mutant and other prostate cancer cell lines and patient-
260 derived xenograft models (PDX)[16]. The SPOP inhibitor increased the protein but not the
261 mRNA levels of established SPOP substrates and ZMNYD11 while the related inactive
262 analog compound 6c did not (Extended Data Fig. 8a-c). The latter did also not exert any
263 activity in 3D culture models (Extended Data Fig. 8d). In agreement with our previous
264 results, we found that *ERG*-fused cells (VCaP, LuCaP-23.1, -35) were more sensitive to
265 SPOP-i than *ERG*-negative cells (22Rv1, LNCaP, PC3), while *SPOP* mutant cells (LuCaP-
266 78, -147) were particularly insensitive in 3D culture models and in xenograft tumor models
267 *in vivo* (Fig. 5a and Extended Data Fig. 8e-j). Strikingly, the sensitivity to SPOP-i *in vivo*
268 correlated well with ERG protein expression levels in the respective *ERG*-fusion positive
269 cell line and PDX model (Fig. 5b). We further validated our results in the mouse prostate
270 epithelial organoids and confirmed the increased sensitivity of ΔERG-expressing cells to
271 SPOP inhibition in this isogenic system (Fig. 5c).

272 Given the notion that wild type SPOP dampens AR function in the context of ERG to
273 sustain tumor growth, we asked if VCaP cells are particularly susceptible to increased DHT
274 levels. Indeed, exposure to high-dose of testosterone *in vivo* or DHT *in vitro* induced
275 similar molecular changes as for the over-expression of mutant SPOP and greatly
276 suppressed the growth of *ERG*-fusion positive cells but not of *SPOP* mutant cells *in vitro*
277 and *in vivo* (Fig. 1c, 5a, d and Extended Data Fig. 9a-i). Moreover, signatures of
278 senescence-associated transcripts were also enriched in VCaP cells upon treatment with

279 DHT, further corroborating our data of a senescence-induced cell cycle arrest (Extended
280 data Fig. 9j). In analogy to SPOP inhibition, the sensitivity to high testosterone *in vivo*
281 correlated very well with ERG protein expression levels in the respective *ERG*-fusion
282 positive cell line and PDX models (Fig. 5b). The data suggests a therapeutic opportunity
283 for SPOP inhibition or high-dose androgen therapy in prostate cancers that express high
284 levels of ERG.

285 Conversely, and because *SPOP* mutant cancers are driven predominantly by androgen
286 signaling and consequently display high-level activation of AR-related transcripts in
287 human tumor tissues, we speculated that these tumors may be particular susceptible to
288 androgen deprivation or anti-androgen therapies (ADT) (Extended Data Fig. 2i). Indeed,
289 the prevalence of *SPOP* mutations in primary tumors -and tumors that had progressed after
290 initial surgery or radiotherapy- is consistently higher as compared to tumors that had
291 become resistant to subsequent ADT (also referred as castration-resistant prostate cancer,
292 CRPC, Extended Data Fig. 9k). In line with the notion that this difference may be related
293 to a better response of SPOP mutant tumors to ADT, SPOP mutant tumor display a trend
294 towards better overall survival despite progressing faster after initial therapy (Extended
295 Data Fig. 9l, m). To functionally analyze the response of androgen deprivation or the anti-
296 androgen enzalutamide, we chose to ectopically expressed different SPOP variants and
297 ΔERG in the androgen-dependent human LAPC4 prostate cancer cells that are wild-type
298 for both driver genes. In accordance with the clinical observation, the presence of mutant
299 SPOP (SPOP-Y87C, SPOP-W131G) rendered LAPC4 cells more susceptible to either
300 ADT or enzalutamide in comparison to cells expressing control vector (Fig. 5e, Extended
301 Data Fig. 9n). In contrast, ΔERG rendered the same cells more resistant to enzalutamide.

302 In line with the previous findings in VCaP and LuCaP-147 cells, ΔERG expression
303 rendered LAPC4 cells susceptible to high levels of DHT, while mutant SPOP had the
304 opposite effect (Extended Data Fig. 9n). Taken together, the different responses to
305 established and experimental therapeutic modalities observed between mutant SPOP and
306 ERG add further credence to their divergent roles of the AR pathway related to
307 tumorigenesis.
308

309 **DISCUSSION**

310 Although multiple studies over recent years have uncovered different genetically-
311 defined subtypes of primary prostate cancer, their biological understanding and therapeutic
312 implications remain largely unexplored territory. Here, we report two diametrically
313 different paths toward tumorigenesis triggered by either highly recurrent missense
314 mutation in *SPOP* or gene fusion involving the *ERG* oncogene. Importantly, wild type
315 SPOP emerges as a critical component that enforces oncogenic ERG signaling in part
316 through dampening AR activity, while mutant SPOP drives tumorigenesis through
317 activation of AR signaling. Moreover, several studies have previously highlighted the
318 importance of AR target genes in the context of SPOP mutants and ERG positive tumors
319 [17,30,31]. Based on the incompatibility between the two tumor subtypes, our work enabled
320 the development of specific custom signatures related to AR and ERG transcript that are
321 necessary to drive proliferation and tumorigenesis in the context of *ERG*-positive and
322 *SPOP*-mutants tumors. In addition, we show that the bromodomain histone reader
323 ZMYND11 is a SPOP substrate implicated downstream of SPOP in the opposing
324 regulation of the ERG and AR pathway in the two tumor subtypes (Extended Data Fig.

325 10a). The AR and ERG pathways have been previously reported to have a partially
326 antagonistic relationship[31,32], further corroborating our findings.

327 Because activation of the androgen receptor by androgens represents a key lineage
328 specific oncogenic pathway in prostate cancer, androgen deprivation/antagonization
329 therapies (ADT) remain the uniform treatment modality up to this very day. That said, the
330 responses to ADT are highly variable and may last from a few weeks up to many years.
331 Here, we provide functional evidence that pre-existing prostate cancer founder mutations
332 influence the treatment response. Most notably, *SPOP* mutations promote susceptibility to
333 androgen deprivations therapies. In agreement with our findings, earlier reports have
334 shown underrepresentation of *SPOP* mutant tumors in cohorts of castration-resistant
335 disease and a more favorable response to the abiraterone and enzalutamide[33,34].

336 Conversely, we show that the presence of the ERG oncogene increases the
337 susceptibility of tumor cells to high-dose androgen therapy, while cells expressing mutant
338 SPOP remain largely unaffected. This is of clinical interest because testosterone treatment
339 of patients with advanced castration-resistant disease has recently shown to trigger anti-
340 tumor responses in around one third of the patients[35]. It is tempting to speculate that these
341 insights may help to discern responders from non-responders.

342 In addition, we provide evidence that the antagonistic relationship between mutant
343 SPOP and ERG may be used towards the development of new therapeutic avenues. More
344 specifically, we show that ERG-driven cancer cells are particularly sensitive to the
345 inhibition of wild-type SPOP using recently developed small molecule inhibitors[16]. Our
346 preclinical data suggests that SPOP inhibition may be effective in clinical settings where
347 ERG is robustly expressed (e.g. neo-adjuvant setting or early metastatic disease).

348 More generally, our results identify another paradigm for antagonistic driver genes in
349 prostate cancer that has recently emerged also for other cancer types [36-38]. In analogy to
350 prostate cancer, truncal point mutations in *DNMT3A* and gene fusions in *PML-RARA* are
351 mutually exclusive drivers in acute myeloid leukemia (AML). Similarly to SPOP, intact
352 DNMT3A has been found to be critical for PML-RARA-driven leukemia (Extended Data
353 Fig. 10b, c) [39,40]. Importantly, we demonstrate here for prostate cancer that the concept of
354 antagonistic driver genes can be exploited to identify therapeutic opportunities.
355

356 **Acknowledgements**

357 We thank the University of Washington and Eva Corey and Donna M. Peehl for
358 providing the Patient-Derived Xenografts (PDX) models. We thank Martina Storz,
359 Susanne Dettwiler, Carmen Gavrisan, and Christiane Mittmann for histology assistance.
360 We thank Enrica-Mira Catò and all members of the IOR/IRB animal core facility for
361 technical assistance and the animal work. In addition, we thank all member of the
362 laboratory for scientific discussions. The results shown here are in whole or part based
363 upon data generated by the TCGA Research Network: https://www.cancer.gov/tcga. J.P.T
364 is funded by a Swiss National Science Foundation Professorship (PP00P3_150645 &
365 PP00P3_179072) grant, and grants by the Swiss Cancer League, the Lega Ticinese contro
366 il cancro, and the Fidinam Foundation. This work was also supported in part by grants from
367 the National Cancer Institute (NCI) Clinical Proteomic Tumor Analysis Consortium grants
368 NIH/NCI U24-CA210986 and NIH/NCI U01 CA214125 (to S.A.C.).
369

370 **Author Contributions**

371 T.B. and J.P.T. originally developed the concept, further elaborated on it and designed
372 the experiments together with G.E.T. and M.B. ; T.B. and G.E.T. performed experiments
373 and analyzed the data together with N.D.U., S.A.C., A.M., T.S., L.P.B., F.S., M.Z., V.C.,
374 Anna R., H.J., D.B., M.C., D.A. and R.G.. T.B. and G.E.T. performed xenograft tumor
375 experiments in immunodeficient mice. Z.D. and C.G.Y. provided SPOP 6b and SPOP 6c
376 compounds. M.S. , S.D. and S.M. performed immunohistochemical experiments and J.P.T
377 the subsequent analysis. H.M. and P.S. provided prostate cancer samples. M.B., A.V. and
378 Andrea R. analyzed genomic and RNA-Seq data. J.P.T, H.M., S.A.C., M. A. R., M.K.J.,
379 A.A., F.B., W.Z. and G.M.C provided funding and resources. J.P.T., T.B., G.E.T. and M.B.
380 interpreted the data and wrote the paper. T.B., G.E.T. and M.B. contributed equally to this
381 work.
382

383 **Author Information**

384 MAR is listed as a co-inventor on US and International patents in the diagnostic and
385 therapeutic fields of ETS gene fusion prostate cancers (Harvard and University of
386 Michigan) and SPOP mutations (Weill Cornell Medicine). JPT has received funding for
387 the venue of scientific conferences from Astellas, MSD, and Janssen/Cilag. The remaining
388 authors declare no competing financial interests. Correspondence and requests for
389 materials should be addressed to J.P.T. (JeanP_Theurillat@ior.iosi.ch)
390

391 **Methods**

392 **Cell culture, Transfection and Infection**

393 VCaP, LNCaP, PC3, 22Rv1, HEK293 cells were purchased from ATCC. LAPC-4 were a
394 gift from Prof. Helmut Klocker. VCaP and HEK293 were grown in DMEM with Glutamax
395 (Gibco); LNCaP, PC3, 22Rv1, LAPC-4 in RPMI medium (Gibco); all were supplemented
396 with 10% full bovine serium (FBS; Invitrogen), or 10% charcoal-stripped serum (CSS;
397 One Shot Fetal Bovine Serum, Charcoal Strippped, Gibco) for androgen deprivation
398 therapy response, and 1% Penicilin/Streptomycin. LuCaP-147 were grown in StemPro
399 medium (hESC SFM StemPro, Gibco) with regular supplements. All cells were incubated
400 at 37°C and 5% CO_2 and routinely tested for mycoplasma contamination.
401 For stable knockdown experiments, cells were infected with pLKO-1 vectors (Sigma) and
402 the following clones were used; *SPOP*: TRCN0000140431 (shSPOP_1) and
403 TRCN000013911 (shSPOP_2); *TRIM24*: TRCN000021262 (shTRIM24_1) and
404 TRCN0000195528 (shTRIM24_2); *ERG*: TRCN0000429354 (shERG_1) and
405 TRCN0000432394 (shERG_2); *ZMYND11*: TRCN0000275479 (shZMYND11_1) and
406 TRCN0000275542 (shZMYND11_2). After infection, cells were selected in the presence
407 of puromycin (2 μg/ml).
408 For SPOP, ΔERG, HA-ZMYND11-WT, HA-ZMYND11-DMT1, HA-ZMYND11-DMT2,
409 MYC and AR over-expression a derivate of the pLX304 vector was used throughout in
410 which the CMV promoter has been exchanged to a PGK promoter and the blasticidin
411 cassette left unchanged (ΔERG constructs) or exchanged by a puromycin resistance
412 cassette (SPOP constructs) (pLX_TRC_307, available at Addgene as Plasmid 41392,
413 pCW107). All ORFs were cloned into pLX_TRC_307 using Nhe1 and Mlu1. Tumors from
414 PDX LuCaP-78, -147, -35,-23.1 were collected, dissociated and cultured as previosly
415 described[41].

416 **Chemicals**

417 MG-132 (M7449) and Cycloheximide (CHX, C4859) were purchased from Sigma and
418 used at 20 μM and 100 μg/ml in all experiments, respectively. SPOP inhibitor (SPOP-i,
419 compound 6b) and its inactive analog (compound 6c), were provided by the laboratory of
420 C. Yang (State Key Laboratory of Drug Research, Shanghai Institute of Materia Medica).
421 DHT (5α-Dihydrotestosterone) was purchased from Sigma (D-073), MDV3100
422 (Enzalutamide) was purchased from APExBIO (A3003). YK-4-279 (ETS inhibitor) was
423 purchased from Selleckchem. All chemicals were used at the indicated concentration.

424

425 **Dose-response curves and cell-growth assays**

426 Cells were seeded (between $1x10^3$ and $1x10^4$ per well) in a 96-well plate. Cells were
427 subsequently treated with serial dilutions of DHT (in 10% CSS medium), or enzalutamide;
428 SPOP inhibitor, ETS inhibitor to determine dose-response curves or were left untreated for
429 cell-growth assays. Proliferation at corresponding time points was assessed by MTT
430 (Methylthiazolyldiphenyl-tetrazolium bromide) assay according to the manufacturer's
431 recommendations (Sigma). For each time point, absorbance (OD, 590 nm) was measured
432 in a microplate reader.

433

434 **Matrigel Invasion assay**

435 Invasion assay was performed as previously described[42]. Briefly, equal number of PC3
436 cells were seeded into 10cm dishes and starved with a medium without fetal bovine serum
437 for 24 hr.; subsequently $1x10^5$ cells were resuspended in 100 μl of starved medium and
438 seeded onto the basement of a Boyden chamber (CLS3422; Sigma) coated with Matrigel.

439 RPMI with 10% fetal bovine serum was added to the lower chamber. After 48hr, invaded
440 cells were fixed with 10% of formalin and stained with crystal violet. Absorbance was
441 measured at 560 nm**.**

442 **Clonogenic assay in methylcellulose**

443 Cells were seeded (between $5x10^3$ and $1x10^4$) in methylcellulose (Methocult H4100,
444 StemCell Technologies) in triplicate. Cells were left untreated for cell-growth assay. For
445 SPOP inhibitor assay, cells were treated with vehicle (0.1% DMSO) or drug (SPOP-i) at
446 corresponding concentration. For androgen therapy, cells were treated with vehicle (0.01%
447 Methanol) or DHT at corresponding concentration. Cells were incubated at 37°C and 5%
448 CO_2 for 7-28 days and colonies were stained with MTT solution at 37°C overnight and
449 absorbance (OD, 590 nm) was measured in a microplate reader.

450

451 **Mouse Prostate Organoid Generation and Experiments**

452 Prostate tissue was extracted from euthanized mice, digested and seeded in matrigel as
453 previously described[43]. To overexpress *SPOP* species and *ΔERG* genes, mouse prostate
454 cells were virally infected by spinoculation for 1hr at 600g at 32 °C and selected with
455 puromycin. For the ‘‘organoid formation assay’’ $1.5x10^4$ single cells were plated per well
456 onto 40µl of Matrigel on day 1 and organoids were grown in “revised human prostate
457 organoids medium” as previously described[41]. Briefly, the medium included the following
458 reagents: adDMEM/F12, glutaMAX (2mM), Pen-strep 100u/ml, HEPES (10mM), B27
459 (1X), EGF (5ng/ml), AB3-01 (500nM), Noggin (100ng/ml), R-Spondin 1 (500ng/ml),
460 DHT (1nM), FGF-2 (5ng/ml), FGF-10 (10ng/ml), Prostaglandin E2 (1000nM). The

461 number of formed organoids that reached 100 μM of diameter was counted on days 14 post
462 plating with cellSens software (Olympus). For the Dose-Response experiment $1x10^4$
463 mouse prostate cells were plated in 40μl of Matrigel and treated with vehicle (0.1% DMSO)
464 or drug (SPOP-i) at indicated concentration for 7 days. Live/dead staining was purchased
465 from Promega (G9711) and performed according to the manufacturer's protocol. The
466 genetically engineered Mouse Prostate Organoids, derived from PbCre;$R26^{F133V}$, were
467 generated as previously described[11].
468

469 **Immunohistochemistry**

470 Cytoblocks were prepared from the pellets of organoids by adding plasma and thrombin in
471 order to obtain a solid matrix. Once solidified, the organoids were fixed in 10% formalin
472 (Thermo Scientific, 5701) and embedded in paraffin as a normal tissue. Sections of 4 μm
473 were used for IHC analyses and hematoxylin and eosin (H&E) staining (Diapath, C0303)
474 and (Diapath, C0363) respectively. Once dried the sections were treated with OTTIX plus
475 solution (Diapath, X0076) and OTTIX shaper solution (Diapath, X0096) to dewax and
476 rehydrate the sections. Antigen retrieval was performed using pH 6 solutions at 98°C for
477 20 min. Successively the endogenous peroxidases and non-specific binding sites were
478 blocked using 3% H2O2 (VWR chemicals, 23615.248) and Protein-Block solution (DAKO
479 Agilent technologies, X0909) respectively, for 10 min. Sections were then stained for anti-
480 p16 (ab211542, Abcam, 1:1200), anti-Ki67 (Clone SP6; Lab Vision Corporation #RT-
481 9106-R7, RTU) and anti-Phospho-HP1y (Ser83) Antibody (CST #2600, 1:200). (. IHC
482 analyses were performed using Imagescope software.
483

484 ***In vivo* experiments**

485 All animal experiments were carried out in male athymic nude mice (Balb/c nu/nu, 6-
486 8 weeks old), NSG mice (NOD Scid Gamma, 6-8 weeks old), and NRG (NOD Rag gamma,
487 6-8 weeks old) accordingly to protocol approved by the Swiss Veterinary Authority (No.
488 TI-14-2014, TI-38-2018, TI-39-2018 and TI-42-2018). Patient-derived xenografts (PDX)
489 LuCaP-147, -78, -35, -23 were provided by Eva Corey (University of Washington) and
490 maintained as previously described[44]. $2x10^6$ VCaP cells, $5x10^6$ LuCaP-147, LuCaP-23.1,
491 LuCaP-35 and LuCaP-78 were resuspended in 100 µl of PBS and Matrigel 1/1 and
492 subcutaneously injected into both of the dorsal flanks of the mice. Tumor growth was
493 recorded using digital caliper and tumor volumes were calculated using the formula ($L \times W$
494 $^2) /2$, where L=length and W=width of tumor. For the testosterone propionate (25mg/kg)
495 and SPOP inhibitor (SPOP-i, 50mg/kg) treatment, the mice were grouped randomly and
496 the treatment started when the mean tumor volume reached $100m^3$. Tumor volume and
497 weight were measured 2 times per week. Testosterone propionate was resuspended first in
498 ethanol (150mg/kg) and then in Corn oil (Sigma) at a final concentration of 25mg/kg. SPOP
499 inhibitor was resuspended in Dulbecco's phosphate buffered saline (PBS) at a final
500 concentration of 50 mg/kg. At the end of the experiment, mice were euthanized, tumors
501 extracted and weighted. Testosterone level was measured using the Human Testosterone
502 ELISA Kit from Abcam (ab174569). In order to recapitulate the levels of
503 supraphysiological testosterone administrated in clinical trials[35], mice reaching at least 3
504 times the testosterone levels measured before the treatment initiated were included in the
505 depicted data.

506 **Antibodies, Immunoblotting, and Immunoprecipiation**

507 Antibodies used in immunoblotting and immunoprecipitation assays were: anti-SPOP
508 (ab81163, Abcam), anti-TRIM24 (Sc-271266, Santa Cruz), anti-ß-ACTIN (4967, Cell
509 Signaling), anti-AR (Sc-7305, Santa Cruz), anti-GADPH (Sc-47724, Santa Cruz), anti-
510 ERG (Sc-271048, Santa Cruz), anti-α-Tubulin (3873S, Cell Signaling), anti-ZMYND11
511 (NBP2-20960, Novus Biologicals), anti-HA (H3663, Sigma), anti-BRD2 (A302-583A,
512 Bethyl Labs), anti-NCOA3 (2126, Cell Signaling), anti-DEK (610948, BDBioscience),
513 anti-p21 (2947S, Cell Signaling) , anti-c-MYC (5605S, Cell Signaling), anti-HOXB13 (Sc-
514 28333, Santa Cruz), anti-PTEN (9559, cell signaling), anti-p21 (ab188224, Abcam), anti-
515 HOXB13 (NBP2-43655, Novus biologicals), anti-GDF-15 (27455-1-AP, proteintech). All
516 antibodies were employed at dilutions suggested by the manufacturers.

517 For immunoblotting, cells were washed with PBS and subsequently lysed in RIPA
518 buffer (Sigma) and sonicated. Protein concentration was determined using the BCA reagent
519 (ThermoFisher), same amounts of protein were separated by SDS-PAGE (Biorad) and
520 transferred onto PVDF membrane (ThermoScientific). The membrane was incubated for
521 one hour in 5% nonfat dry milk/TBS-T blocking buffer followed by incubation with the
522 primary antibody overnight at 4°C. The membrane was washed with TBS-T followed by
523 incubation with horseradish peroxidase-conjugated secondary antibody (Promega).

524 To detect interactions of SPOP and ZMYND11, cells were lysed in 1 % NP40 buffer
525 (50mM Tris-HCl pH 7.4, 150 mM NaCl, 1 % NP40) with 2x protease inhibitor cocktail
526 (Complete, Roche), sonicated, and 3 mg of lysate were incubated overnight with 2 μg of
527 anti-HA-tag or control mouse IgG antibody (sc-2025, Santa Cruz Biotechnology) at 4 °C.
528 Subsequently, antibodies were collected by 25 μl protein A/G magnetic beads (88803,

529 Fisher Scientific) for 2h, followed by 2 washing steps with 1 % NP40 buffer. Proteins were
530 eluted by addition of 1x SDS-sample buffer under reducing conditions at 95 °C for 5 min.

531 ***In Vivo* Ubiquitylation Assay**

532 293T cells were transiently transfected with indicated plasmids: pCW107-HA-
533 ZMYND11-WT or HA-ZYMND11-DMT1/DMT2 (2 μg), pCW107-SPOP-WT or SPOP-
534 MT (2 μg), CMV-8x Ubi-His (2 μg). 42 hours later, cells were treated with MG-132
535 (20μM) or DMSO for additional 7 hours. Cells were then washed with PBS and collected
536 by centrifugation. Small amount of cells was lysed in RIPA buffer and the rest in Buffer C
537 (6M guanidine –HCL, 0.1 M Na2HPO4/NaH2PO4, 10mM Imidazole, pH=8). The whole
538 cells extract was sonicated and incubated with 60 μl of Ni-NTA agarose (Sigma) overnight
539 at 4°C. Next, Ni-NTA beads were washed once with Buffer C, twice with Buffer D (1
540 volume of Buffer C: 3 volumes of Buffer E) and once with Buffer E (25 mMTris-HCL, 20
541 mM Imidazole, pH=6.8). Elution of bound proteins was processed by boiling in 1x SDS
542 loading buffer containing 300 mM Imidazole. Samples were loaded, separated by SDS-
543 PAGE, and detected by immunoblotting.

544

545 **Gene Expression Studies**

546 RNA was extracted using the RNeasy kit (Qiagen) and processed by Kapa SybrFAST
547 one-Step qRT-PCR kit according to manufacturer`s instructions. qRT-PCR was undertaken
548 on an Applied Biosystems StepOnePlus System. The target mRNA expression was
549 quantified using ΔΔCt method and normalized to Actin expression. The following primers
550 were used: *SPOP*, forward 5'- GAAATGGTGTTTGCGAGTAAACC-3', reverse 5`-

551 TACCTACGCTTCCAGTCTCTG-3'; *ERG*, forward 5'-
552 TGTATGCCAGCATTTGTTTCTT-3', reverse 5'- TTGCTGGTCTTGCCATTCCT-3';
553 *β-ACTIN,* forward 5'-AAGGAGCCCCACGAAAAAT-3', reverse 5'-
554 ACCGAACTTGCATTGATTCCAG-3'; *PLAU,* forward 5'-
555 TACGGCTCTGAAGTCACCACCAAAAT-3', reverse 5'-
556 CCCCAGCTCACAATTCCAGTCAA-3'; *PLAT,* forward 5'-
557 CACTGGGCCTGGGCAAACATA-3', reverse 5'-CACGTCAGCCTGCGGTTCTTC-3';
558 *TMPRSS2,* forward 5'-CAGGAGTGTACGGGAATGTGATGGT-3', reverse 5'-
559 GATTAGCCGTCTGCCCTCATTTGT-3'; *KLK2*, forward 5'- CTGCCCATTGCCTAA
560 AGAAG-3', reverse 5'- GTAGAGCGGGTGTGGGAAG-3'; *PSA* forward 5'-
561 GAGCACCCCTATCAACCCCCTATT -3' , reverse 5'-
562 AGCAACCCTGGACCTCACACCTAA-3'; *ZMYND11,* forward 5'-
563 ATGGCACGTTTAACAAAAAGACG-3', reverse 5'-
564 CGGTCAATGTTGGCAATCTGC-3'; *BRD2*, forward 5'-
565 CTACGTAAGAAACCCCGGAAG-3′, reverse 5'-GCTTTTTCTCCAAAGCCAGTT-3;
566 *TRIM24*, forward 5`-CAGCCACAAATGCCTAAGCAG-3 ′ , reverse 5'-
567 GTGTTGGGAACTTGGATAACTGG-3; *NCOA3*, forward 5'-
568 AGACGGGAGCAGGAAAGTAAA-3', reverse 5'-
569 GTAAAAGCGGTCCTAAGGAGTC-3'; *DEK*, forward 5'-
570 AACTGCTTTACAACAGGCCAG-3' , reverse 5'-ATGGTTTGCCAGAAGGCTTTG-
571 3'.
572

573 **RNA-Seq of VCaP, LNCaP and LuCaP cells**

574 RNA sequencing for all experiments involving LuCaP xenografts, VCaP and LNCaP
575 cells was performed at the Institute of Oncology Research using Next Ultra II Directional
576 RNA Library Prep Kit for Illumina and sequenced on the Illumina NextSeq500 with single-
577 end, 75 base pair long reads. The overall quality of sequencing reads was evaluated using
578 a variety of tools, namely FastQC (Andrews S., 2010), RSeQC[45], AfterQC[46] and
579 Qualimap[47]. Sequence alignments to the reference human genome (GRCh38) was
580 performed using STAR [48] (v.2.5.2a). Gene-expression was quantified at gene level by using
581 the comprehensive annotations made available by Gencode[49]. Specifically, we used *v27*
582 release of the Gene Transfer File (GTF). Raw-counts were further processed in the *R*
583 Statistical environment and downstream differential expression analysis was performed
584 using the DESeq2[50] pipeline.

585 Genes being expressed at very low levels were automatically filtered out through the
586 *Independent Filtering* feature embedded in DESeq2 (alpha = 0.05). Differential-expression
587 results were ranked according to the computed Wald-statistics values. Subsequently, gene-
588 set enrichment testing was performed using Camera[51] pre-ranked (inter-gene correlation
589 equal to 0.1, parametric test procedure). Statistical enrichments were assessed for gene-sets
590 belonging to the Hallmark collection, which is curated by the Molecular Signature
591 DataBase[52,53] (*MSigDB*), and for custom ERG and DHT-specific gene-signatures. All
592 enrichments were corrected for multiple testing using Benjamini and Hochberg FDR
593 adjusted p-value.

594

595 **Identification of ERG and AR related gene signatures**

596 We retrieved RNA-seq data from GEO Dataset *GSE83652*[14] to identify transcriptional
597 perturbations in VCaP cells following treatment with DHT or following silencing of ERG.
598 To this purpose we completely reprocessed samples SRR3713255-57, SRR3713267-72
599 using *STAR* and *DESeq2* as previously described for VCaP cells. In addition, to identify
600 direct targets, we integrated information relative to AR and ERG chromatin binding sites,
601 which we derived from GEO Dataset *GSE28950*[25]. To maximize the number of peaks and
602 to reduce false negatives, we merged results of experiments performed at different time
603 points, namely 2h and 18h after DHT exposure. De-multiplexed reads were aligned to *hg38*
604 release of the human reference genome using bwa-mem[54] (0.7.15). MACS[55] (v.2.1.0) was
605 used to perform peak calling procedure using a cutoff FDR q-value of 0.01 and a mappable
606 genome size optimized for *hg38* equal to 2.9 gigabases. Downstream analysis was
607 performed in R statistical environment. We identified binding sites overlapping promoters
608 by using bedtools[56].
609 Promoters were defined as DNA regions ranging from 1500 *bp* upstream to 500 *bp*
610 downstream of Transcription Start Sites (TSSs).
611 To discriminate between ERG- and AR- specific transcriptional responses we stratified
612 genes into three main classes: genes whose promoter regions are bound by *AR* but not by
613 *ERG*, genes whose promoters are bound by ERG but not by *AR*, and finally, genes whose
614 promoters are co-bound by both AR and ERG. AR bound only genes were further
615 subdivided into two sets, those being significantly (FDR<0.05) induced following DHT
616 treatment and those being significantly repressed. A similar approach was applied to ERG
617 bound only genes, where genes were subdivided into ERG-induced and ERG-repressed
618 gene-sets, if they were respectively down or up-regulated following *ERG* silencing. To be

619 more stringent in the definition of AR-specific and ERG-specific signatures, we excluded
620 genes from the ERG-induced set that were also significantly up-regulated following DHT
621 treatment, *vice-versa* we excluded ERG-repressed genes that were significantly down-
622 regulated following DHT-treatment. The same criteria were applied for DHT-specific
623 gene-sets. Finally, defined an additional gene-set (DHT-induced/ERG-repressed)
624 consisting of genes being co-bound by AR and ERG in their promoter region, which were
625 significantly up-regulated following DHT treatment but also significantly upregulated
626 following ERG-silencing. All gene-sets are detailed in Supplementary Table 1. Overlap
627 between custom derived gene-signatures and the most represented Hallmark's gene-sets
628 was assessed using GeneOverlap R package (Shen L, Sinai M, 2013). Two-dimensional
629 network visualization was generated with Cytoscape. [57]
630

631 **Gene-set testing and RNA-Seq data processing of clinical samples**

632 Publicly available RNA-Seq data for primary prostate cancer were obtained from The
633 Caner Genome Atlas[3] (TCGA) database and retrieved from Genomics Data Commons
634 (GDC) in form of gene-centric raw counts, using *TCGAbiolinks* package[58]. We selected
635 individuals characterized by either SPOP or ERG fusion, and a third group defined as
636 "others", which includes all remaining samples, excluding those patients exhibiting any
637 other ETS-rearrangement. Differential expression and gene-set enrichment between
638 samples harboring ERG fusions and SPOP-mutations were performed using *DESeq2* and
639 *Camera* (pre-ranked) as previously described for prostate cancer cells. Single-sample gene-
640 set enrichment analysis (GSVA[59] package) was applied to measure, for each individual
641 patient, the overall activity of the custom gene-sets that were previously generated in VCaP

642 cells. Following differential expression analysis between ERG-rearranged and SPOP
643 mutant primary tumors, we defined two gene-sets consisting of SPOP-upregulated (n =
644 443, $\log_2$FC >1, FDR<0.05) and ERG-upregulated (n = 359, $\log_2$FC >1, FDR<0.05) genes.
645 *PolyA+* RNASeq data for metastatic prostate cancer were obtained from SU2C
646 cohort[60]. Normalized *RPKM* values, retrieved through *cBioportal*, were log transformed
647 and patient's categorization (SPOP/ERG/OTHER) was performed in the same manner as
648 for primary tumors. To evaluate whether transcriptional differences occurring between
649 ERG-rearranged and SPOP-mutant individuals were also conserved in CRPC setting, we
650 quantified the above mentioned SPOP-upregulated/ERG-upregulated signatures in the
651 SU2C 2019 cohort, using single-sample gene-set enrichment analysis. The obtained
652 ssGSEA scores were scaled in a range between -1 and 1 (SPOP-Upregulated) and between
653 1 and -1 (ERG-upregulated, inverted). Subsequently we averaged these rescaled values in
654 order to obtain an aggregate score.
655
656 **Circular representation of interactions between gene-sets**
657 Chord diagrams were generated using circlize[61] package in R statistical environment.
658 Strings, whose thickness is proportional to the number of shared elements, represent
659 common genes between sets.
660
661 **ZMYND11 ChIP-seq in VCaP cells**
662 ChIP-seq using anti-ZMYND11 antibody (NBP2-20960, Novus Biologicals) was
663 performed in VCaP cells, overexpressing either wild-type SPOP or mutant SPOP harboring
664 Y87C point mutation. Briefly, to isolate chromatin, cells (120.000.000 per IP) were cross-

665 linked using 1% Formaldehyde cross-link protein-DNA complexes and crosslinking was
666 terminated by the addition of 1/10 volume 1.25 M glycine for 5 min at room temperature
667 followed by cell lysis and sonication, resulting in an average chromatin fragment size of
668 200 bp. Samples lysis was performed as previously described using MNase enzyme 1000
669 gel units=1 uL[62]. After adding the MNase sonication buffer, the samples were sonicated
670 for 30 cycles, 30 sec ON and 30 sec OFF at high voltage. ChIP and input DNA (50 ng)
671 were used for indexed library preparation using NEBNext Ultra II DNA Library Prep kit
672 and subjected to 75 *bp* single-end sequencing on the Illumina NextSeq500. All procedures
673 were performed at the Institute of Oncology Research. De-multiplexed reads were aligned
674 to *hg38* release of the human reference genome using bwa-mem[54] (0.7.15). MACS[55]
675 (v.2.1.0) was used to perform peak calling procedure using a cutoff FDR q-value of 0.01
676 and a mappable genome size optimized for *hg38* equal to 2.9 gigabases. Downstream
677 analysis was performed in R statistical environment. ChIPseeker[63] was used to annotate
678 peaks and to represent the distribution of ZMYND11 binding sites relative to Transcription
679 Start Sites (TSSs). The R package chipenrich[64] was subsequently used to determine
680 enrichment or depletion of ZMYND11 peaks in regions surrounding *TSSs* of genes that are
681 included in Hallmarks or custom gene-set collections. Surrounding regions were defined
682 as ranging from 5kb upstream to 5kb downstream of their *TSSs* (locusdef = 5kb), which is
683 in line with the overall behavior of ZMYND11 binding sites around *TSSs* (Extended Data
684 Fig. 6f-g).
685

686 **Identification of AR-binding sites in primary prostate cancer specimen**

687 Publicly available ChIP-Seq data were retrieved from GSE120738[3]. ChIP-seq data were
688 reprocessed as described for ZMYND11 samples. Differential binding affinity of AR
689 between ERG-rearranged and SPOP-mutant tumors was performed using DiffBind (Stark
690 R and Brown G, 2011).
691

692 **Frequency of SPOP mutations across patients' cohorts**

693 We defined the percentage of SPOP-mutant and TMPRSS2-ERG positive tumors
694 across different patients' cohorts originating from multiple sources. Patients with
695 primary/loco-regional prostate tumors were derived from TCGA and MSK-IMPACT
696 Clinical Sequencing cohorts[34]. Patients with tumor-progression (non-castrate) were
697 derived from MSK-IMPACT and TCGA cohorts, by including from the latter only
698 individuals that showed tumor-progression based on survival information. Castration
699 resistant prostate cancer patients were retrieved from MSK-IMPACT, Beltran et. al[65] and
700 from the SU2C[60] .datasets. Neuroendocrine prostate cancer samples were retrieved from
701 the SU2C cohort (samples annotated with neuroendocrine features) and from Beltran et
702 al[65]. Total number of *SPOP*-mutant and *TMPRSS2-ERG* tumors were determined based
703 on the clinical annotations of the individual studies and integrated with fusion information
704 from TCGA Fusion Gene Database (www.tumorfusions.org). Survival analysis was
705 performed in R statistical environment using the TCGA and MSK-IMPACT clinical
706 sequencing cohort.
707

708 **Quantitative liquid-chromatography-mass spectrometry (LC-MS/MS)**

709 In solution digestion VCaP cell pellets were lysed at 4 ºC in 8 M urea, 50 mM Tris-
710 HCl pH 8.0, 150 mM NaCl, 1 mM EDTA, 2 µg/µl aprotinin (Sigma-Aldrich), 10 µg/µl
711 leupeptin (Roche), and 1 mM phenylmethylsulfonyl fluoride (PMSF) (Sigma). Protein
712 concentration was determined using a bicinchoninic acid (BCA) protein assay (Pierce).
713 Proteins were reduced with 5 mM (DTT) for 45 min at room temperature (RT), followed
714 by alkylation with 10 mM iodoacetamide for 30 min at room temperature in the dark. The
715 urea concentration was reduced to 2 M using 50 mM Tris-HCl, pH 8. Samples were
716 digested for 2 h at 25 ºC with endoproteinase Lys-C (Wako Laboratories) at an enzyme-to-
717 substrate ratio of 1:50. Samples were subsequently digested overnight at 25 ºC with
718 sequencing grade trypsin (Promega) at an enzyme-to-substrate ratio of 1:50. Following
719 overnight digestion, samples were acidified to a final concentration of 1% formic acid.
720 Peptide samples were desalted on a 100 mg tC18 Sep-Pak SPE cartridge (Waters).
721 Cartridges were conditioned with 1 mL of 100% MeCN, 1 mL of 50% MeCN/0.1% FA,
722 and 4x with 1 mL of 0.1% TFA. The sample was loaded, and washed 3x with 1 mL of 0.1%
723 TFA, 1x with 1 mL of 1% FA, and eluted 2x with 600 µl of 50% MeCN/0.1% FA.
724
725 **TMT labeling of peptides**
726 Peptides were labeled with TMT 10-plex isobaric mass tagging reagents (Thermo
727 Fisher Scientific). Each TMT reagent was resuspended in 41 µL of MeCN. Peptides were
728 resuspended in 100 µL of 50 mM HEPES and combined with TMT reagent. Samples were
729 incubated at RT for 1 h while shaking. The TMT reaction was quenched with 8 µL of 5%
730 hydroxylamine at RT for 15 min with shaking. TMT labeled samples were combined, dried

731 to completion, reconstituted in 100 µL of 0.1% FA, and desalted on StageTips or 100 mg
732 SepPak columns as described above.
733
734 **Basic Reverse Phase (bRP) Fractionation**
735 The TMT labeled samples were fractionated using offline high pH reversed-phase
736 chromatography (bRP) as previously described [Mertins et al Nat Prot]. Samples were
737 fractionated using Zorbax 300 Extend C18 column (4.6 × 250 mm, 300 Å, 5 µm, Agilent)
738 on an Agilent 1100 series high-pressure liquid chromatography (HPLC) system. Samples
739 were reconstituted in 900 µL of 4.5 mM ammonium formate (pH 10) in 2% (vol/vol)
740 acetonitrile (MeCN) (bRP solvent A). Samples were injected with Solvent A at a flow rate
741 of 1 mL/min and separated using a 96 min gradient. The gradient consisted of an initial
742 increase to 16% solvent B (90% MeCN, 5 mM ammonium formate, pH 10), followed by
743 60 min linear gradient from 16% solvent B to 40% B and successive ramps to 44% and
744 60% at a flow rate of 1 mL/min. Fractions were collected in a 96-deep well plate (GE
745 Healthcare) and pooled in a non-contiguous manner into final 24 proteome fractions.
746 Pooled fractions were dried to completeness using a SpeedVac concentrator.
747
748 **Liquid chromatography and mass spectrometry**
749 Desalted peptides were resuspended in 3% MeCN/0.1% FA and analyzed by online
750 nanoflow liquid chromatography tandem mass spectrometry (LC-MS/MS) using Q-
751 Exactive plus mass spectrometer (Thermo Fisher Scientific) coupled on-line to a Proxeon
752 Easy-nLC 1200 as previously described [Mertins et al Nature Protocols]. Briefly, 1 ug of
753 each sample was loaded onto a microcapillary column (360 µm outer diameter × 75 µm

754 inner diameter) containing an integrated electrospray emitter tip (10 µm), packed to
755 approximately 22 cm with ReproSil-Pur C18-AQ 1.9 µm beads (Dr. Maisch GmbH) and
756 heated to 50 °C. Samples were analyzed with 110 min LC-MS method. The 110 min
757 method contained a mobile phase with a flow rate of 200 nL/min, comprised of 3%
758 acetonitrile/0.1% formic acid (Solvent A) and 90% acetonitrile/0.1% formic acid (Solvent
759 B), with the following gradient profile: (min:%B) 0:2; 1:6; 85:30; 94:60; 95:90; 100:90;
760 101:50; 110:50 (the last two steps at 500 nL/min flow rate). The Q-Exactive plus MS was
761 operated in the data-dependent mode acquiring HCD MS/MS scans (r =35,000) after each
762 MS1 scan (r = 70,000) on the 12 most abundant precursor ions using an MS1 target of 3 ×
763 10^6 and an MS2 target of 5 × 10^4 . The maximum ion time utilized for MS/MS scans
764 was 120 ms; the HCD-normalized collision energy was set to 30; the dynamic exclusion
765 time was set to 20 s, isotope exclusion function was enabled, and peptide match function
766 was set to preferred. Charge exclusion was enabled for charge states that were unassigned,
767 1 and >6.
768
769 **MS Data Analysis**
770 All data were analyzed using Spectrum Mill software package v 6.1 pre-release
771 (Agilent Technologies). Similar MS/MS spectra acquired on the same precursor m/z within
772 +/- 60 s were merged. MS/MS spectra were excluded from searching if they were not
773 within the precursor MH+ range of 750-4000 Da or if they failed the quality filter by not
774 having a sequence tag length >0. MS/MS spectra were searched against UniProt human

775 database. All spectra were allowed +/- 20 ppm mass tolerance for precursor and product
776 ions, 30% minimum matched peak intensity, and "trypsin allow P" enzyme specificity with
777 up to 4 missed cleavages. The fixed modifications were carbamidomethylation at cysteine,
778 and TMT at N-termini and internal lysine residues. Variable modifications included
779 oxidized methionine and N-terminal protein acetylation. Individual spectra were
780 automatically designated as confidently assigned using the Spectrum Mill autovalidation
781 module. Specifically, a target-decoy based false-discovery rate (FDR) scoring threshold
782 criteria via a two-step auto threshold strategy at the spectral and protein levels was used.
783 First, peptide mode was set to allow automatic variable range precursor mass filtering with
784 score thresholds optimized to yield a spectral level FDR of 1 %. A protein polishing
785 autovalidation was applied to further filter the peptide spectrum matches using a target
786 protein-level FDR threshold of 0. Following autovalidation, a protein-protein comparison
787 table was generated, which contained experimental ratios. For all experiments, non-human
788 contaminants and reversed hits were removed. Furthermore, data were filtered to only
789 consider proteins with 2 or more unique peptides and was median normalized.
790

791 **Statistical analysis**

792 GraphPad Prism version 8.3 (GraphPad Software) was used for statistical analysis.
793 Data are depicted as mean + s.e.m. unless otherwise specified. The number of independent
794 experiments or mice used is indicated in each figure legends. Unpaired Student's t-test was
795 used for comparisons between two groups, one-way analysis of variance (ANOVA) with
796 multiple comparisons for two groups or more, and two-way ANOVA with multiple
797 comparisons for repeated measurements. Multiple comparisons tests were corrected by

controlling the False Discovery Rate (FDR) using Benjamini and Hochberg's method. . Correlation analyses were performed using Pearson correlation coefficients.

Data Availability

The original mass spectra have been deposited in the public proteomics repository MassIVE and are accessible at ftp://MSV000082915@massive.ucsd.edu when providing the dataset password: prostate. If requested, also provide the username: MSV000082915. This data will be made public upon acceptance of the manuscript.

RNA-Seq data generated have been deposited in the *ArrayExpress* database at EMBL-EBI and were assigned the accessions *E-MTAB-7165, E-MTAB-7170, E-MTAB-7173*. These data are accessible when providing the datasets username and password as follow:

Username: *Reviewer_E-MTAB-7165* Password: *4sJqpicv*

Username: *Reviewer_E-MTAB-7170* Password: *AAA65MMy*

Username: *Reviewer_E-MTAB-7173* Password*: sIpcob0o*.

CHiP-Seq data generated have been deposited in the *ArrayExpress* database at EMBL-EBI and were assigned the accessions *E-MTAB-7174*. These data are accessible when providing the dataset username and password as follow:

Username: *Reviewer_E-MTAB-7174* Password: *onwwwwni*

All these data will be made public upon acceptance of the manuscript.

References

1 Mina, M. *et al.* Conditional Selection of Genomic Alterations Dictates Cancer Evolution and Oncogenic Dependencies. *Cancer cell* **32**, 155-168.e156, doi:10.1016/j.ccell.2017.06.010 (2017).

2 Davies, H. *et al.* Mutations of the BRAF gene in human cancer. *Nature* **417**, 949-954, doi:10.1038/nature00766 (2002).

825 3 TCGA. The Molecular Taxonomy of Primary Prostate Cancer. *Cell* **163**, 1011-
826 1025, doi:10.1016/j.cell.2015.10.025 (2015).
827 4 Barbieri, C. E. *et al.* Exome sequencing identifies recurrent SPOP, FOXA1 and
828 MED12 mutations in prostate cancer. *Nature genetics* **44**, 685-689,
829 doi:10.1038/ng.2279 (2012).
830 5 Baca, S. C. *et al.* Punctuated evolution of prostate cancer genomes. *Cell* **153**,
831 666-677, doi:10.1016/j.cell.2013.03.021 (2013).
832 6 Robinson, D. *et al.* Integrative clinical genomics of advanced prostate cancer.
833 *Cell* **161**, 1215-1228, doi:10.1016/j.cell.2015.05.001 (2015).
834 7 Grasso, C. S. *et al.* The mutational landscape of lethal castration-resistant
835 prostate cancer. *Nature* **487**, 239-243, doi:10.1038/nature11125 (2012).
836 8 Gan, W. *et al.* SPOP Promotes Ubiquitination and Degradation of the ERG
837 Oncoprotein to Suppress Prostate Cancer Progression. *Molecular cell* **59**, 917-
838 930, doi:10.1016/j.molcel.2015.07.026 (2015).
839 9 An, J. *et al.* Truncated ERG Oncoproteins from TMPRSS2-ERG Fusions Are
840 Resistant to SPOP-Mediated Proteasome Degradation. *Molecular cell* **59**, 904-
841 916, doi:10.1016/j.molcel.2015.07.025 (2015).
842 10 Shoag, J. *et al.* SPOP mutation drives prostate neoplasia without stabilizing
843 oncogenic transcription factor ERG. *The Journal of clinical investigation*,
844 doi:10.1172/JCI96551 (2017).
845 11 Blattner, M. *et al.* SPOP Mutation Drives Prostate Tumorigenesis In Vivo
846 through Coordinate Regulation of PI3K/mTOR and AR Signaling. *Cancer cell*
847 **31**, 436-451, doi:10.1016/j.ccell.2017.02.004 (2017).
848 12 King, J. C. *et al.* Cooperativity of TMPRSS2-ERG with PI3-kinase pathway
849 activation in prostate oncogenesis. *Nature genetics* **41**, 524-526,
850 doi:10.1038/ng.371 (2009).
851 13 Carver, B. S. *et al.* Aberrant ERG expression cooperates with loss of PTEN to
852 promote cancer progression in the prostate. *Nature genetics* **41**, 619-624,
853 doi:10.1038/ng.370 (2009).
854 14 Bose, R. *et al.* ERF mutations reveal a balance of ETS factors controlling
855 prostate oncogenesis. *Nature* **546**, 671-675, doi:10.1038/nature22820
856 (2017).
857 15 Saar, M. *et al.* Spheroid culture of LuCaP 147 as an authentic preclinical model
858 of prostate cancer subtype with SPOP mutation and hypermutator phenotype.
859 *Cancer letters* **351**, 272-280, doi:10.1016/j.canlet.2014.06.014 (2014).
860 16 Guo, Z. Q. *et al.* Small-Molecule Targeting of E3 Ligase Adaptor SPOP in Kidney
861 Cancer. *Cancer cell* **30**, 474-484, doi:10.1016/j.ccell.2016.08.003 (2016).
862 17 Geng, C. *et al.* Androgen receptor is the key transcriptional mediator of the
863 tumor suppressor SPOP in prostate cancer. *Cancer research* **74**, 5631-5643,
864 doi:10.1158/0008-5472.Can-14-0476 (2014).
865 18 Geng, C. *et al.* Prostate cancer-associated mutations in speckle-type POZ
866 protein (SPOP) regulate steroid receptor coactivator 3 protein turnover.
867 *Proceedings of the National Academy of Sciences of the United States of America*
868 **110**, 6997-7002, doi:10.1073/pnas.1304502110 (2013).

869 19 An, J., Wang, C., Deng, Y., Yu, L. & Huang, H. Destruction of full-length androgen
870 receptor by wild-type SPOP, but not prostate-cancer-associated mutants. *Cell*
871 *reports* **6**, 657-669, doi:10.1016/j.celrep.2014.01.013 (2014).
872 20 Theurillat, J. P. *et al.* Prostate cancer. Ubiquitylome analysis identifies
873 dysregulation of effector substrates in SPOP-mutant prostate cancer. *Science*
874 *(New York, N.Y.)* **346**, 85-89, doi:10.1126/science.1250255 (2014).
875 21 Groner, A. C. *et al.* TRIM24 Is an Oncogenic Transcriptional Activator in
876 Prostate Cancer. *Cancer cell*, doi:10.1016/j.ccell.2016.04.012 (2016).
877 22 Zhang, P. *et al.* Intrinsic BET inhibitor resistance in SPOP-mutated prostate
878 cancer is mediated by BET protein stabilization and AKT-mTORC1 activation.
879 *Nature medicine* **23**, 1055-1062, doi:10.1038/nm.4379 (2017).
880 23 Janouskova, H. *et al.* Opposing effects of cancer-type-specific SPOP mutants on
881 BET protein degradation and sensitivity to BET inhibitors. *Nature medicine* **23**,
882 1046-1054, doi:10.1038/nm.4372 (2017).
883 24 Dai, X. *et al.* Prostate cancer-associated SPOP mutations confer resistance to
884 BET inhibitors through stabilization of BRD4. *Nature medicine* **23**, 1063-1071,
885 doi:10.1038/nm.4378 (2017).
886 25 Chng, K. R. *et al.* A transcriptional repressor co-regulatory network governing
887 androgen response in prostate cancers. *The EMBO journal* **31**, 2810-2823,
888 doi:10.1038/emboj.2012.112 (2012).
889 26 Hernandez-Segura, A. *et al.* Unmasking Transcriptional Heterogeneity in
890 Senescent Cells. *Curr Biol* **27**, 2652-2660.e2654,
891 doi:10.1016/j.cub.2017.07.033 (2017).
892 27 Purcell, M., Kruger, A. & Tainsky, M. A. Gene expression profiling of replicative
893 and induced senescence. *Cell cycle (Georgetown, Tex.)* **13**, 3927-3937,
894 doi:10.4161/15384101.2014.973327 (2014).
895 28 Wen, H. *et al.* ZMYND11 links histone H3.3K36me3 to transcription elongation
896 and tumour suppression. *Nature* **508**, 263-268, doi:10.1038/nature13045
897 (2014).
898 29 Mani, R. S. *et al.* TMPRSS2-ERG-mediated feed-forward regulation of wild-type
899 ERG in human prostate cancers. *Cancer research* **71**, 5387-5392,
900 doi:10.1158/0008-5472.CAN-11-0876 (2011).
901 30 Chen, Y. *et al.* ETS factors reprogram the androgen receptor cistrome and
902 prime prostate tumorigenesis in response to PTEN loss. *Nature medicine* **19**,
903 1023-1029, doi:10.1038/nm.3216 (2013).
904 31 Yu, J. *et al.* An integrated network of androgen receptor, polycomb, and
905 TMPRSS2-ERG gene fusions in prostate cancer progression. *Cancer cell* **17**,
906 443-454, doi:10.1016/j.ccr.2010.03.018 (2010).
907 32 Mounir, Z. *et al.* ERG signaling in prostate cancer is driven through PRMT5-
908 dependent methylation of the Androgen Receptor. *eLife* **5**,
909 doi:10.7554/eLife.13964 (2016).
910 33 Boysen, G. *et al.* SPOP-Mutated/CHD1-Deleted Lethal Prostate Cancer and
911 Abiraterone Sensitivity. *Clinical cancer research : an official journal of the*
912 *American Association for Cancer Research*, doi:10.1158/1078-0432.ccr-18-
913 0937 (2018).

34 Abida, W. *et al.* Prospective Genomic Profiling of Prostate Cancer Across Disease States Reveals Germline and Somatic Alterations That May Affect Clinical Decision Making. *JCO Precis Oncol* **2017**, doi:10.1200/PO.17.00029 (2017).

35 Teply, B. A. *et al.* Bipolar androgen therapy in men with metastatic castration-resistant prostate cancer after progression on enzalutamide: an open-label, phase 2, multicohort study. *The Lancet. Oncology* **19**, 76-86, doi:10.1016/S1470-2045(17)30906-3 (2018).

36 Zhao, D. *et al.* Synthetic essentiality of chromatin remodelling factor CHD1 in PTEN-deficient cancer. *Nature* **542**, 484-488, doi:10.1038/nature21357 (2017).

37 Lee, S. C. *et al.* Synthetic Lethal and Convergent Biological Effects of Cancer-Associated Spliceosomal Gene Mutations. *Cancer cell* **34**, 225-241.e228, doi:10.1016/j.ccell.2018.07.003 (2018).

38 Zeineldin, M. *et al.* MYCN amplification and ATRX mutations are incompatible in neuroblastoma. *Nat Commun* **11**, 913, doi:10.1038/s41467-020-14682-6 (2020).

39 Cole, C. B. *et al.* PML-RARA requires DNA methyltransferase 3A to initiate acute promyelocytic leukemia. *The Journal of clinical investigation* **126**, 85-98, doi:10.1172/jci82897 (2016).

40 Ley, T. J. *et al.* Genomic and epigenomic landscapes of adult de novo acute myeloid leukemia. *The New England journal of medicine* **368**, 2059-2074, doi:10.1056/NEJMoa1301689 (2013).

41 Beshiri, M. L. *et al.* A PDX/Organoid Biobank of Advanced Prostate Cancers Captures Genomic and Phenotypic Heterogeneity for Disease Modeling and Therapeutic Screening. *Clin Cancer Res* **24**, 4332-4345, doi:10.1158/1078-0432.CCR-18-0409 (2018).

42 Tomlins, S. A. *et al.* Distinct classes of chromosomal rearrangements create oncogenic ETS gene fusions in prostate cancer. *Nature* **448**, 595-599, doi:10.1038/nature06024 (2007).

43 Drost, J. *et al.* Organoid culture systems for prostate epithelial and cancer tissue. *Nature protocols* **11**, 347-358, doi:10.1038/nprot.2016.006 (2016).

44 Corey, E. *et al.* LuCaP 35: a new model of prostate cancer progression to androgen independence. *Prostate* **55**, 239-246, doi:10.1002/pros.10198 (2003).

45 Wang, L., Wang, S. & Li, W. RSeQC: quality control of RNA-seq experiments. *Bioinformatics (Oxford, England)* **28**, 2184-2185, doi:10.1093/bioinformatics/bts356 (2012).

46 Chen, S. *et al.* AfterQC: automatic filtering, trimming, error removing and quality control for fastq data. *BMC Bioinformatics* **18**, 80, doi:10.1186/s12859-017-1469-3 (2017).

47 Garcia-Alcalde, F. *et al.* Qualimap: evaluating next-generation sequencing alignment data. *Bioinformatics (Oxford, England)* **28**, 2678-2679, doi:10.1093/bioinformatics/bts503 (2012).

48 Dobin, A. *et al.* STAR: ultrafast universal RNA-seq aligner. *Bioinformatics (Oxford, England)* **29**, 15-21, doi:10.1093/bioinformatics/bts635 (2013).

960 49 Harrow, J. *et al.* GENCODE: the reference human genome annotation for The
961 ENCODE Project. *Genome research* **22**, 1760-1774,
962 doi:10.1101/gr.135350.111 (2012).
963 50 Love, M. I., Huber, W. & Anders, S. Moderated estimation of fold change and
964 dispersion for RNA-seq data with DESeq2. *Genome biology* **15**, 550,
965 doi:10.1186/s13059-014-0550-8 (2014).
966 51 Wu, D. & Smyth, G. K. Camera: a competitive gene set test accounting for inter-
967 gene correlation. *Nucleic acids research* **40**, e133, doi:10.1093/nar/gks461
968 (2012).
969 52 Liberzon, A. *et al.* The Molecular Signatures Database (MSigDB) hallmark gene
970 set collection. *Cell Syst* **1**, 417-425, doi:10.1016/j.cels.2015.12.004 (2015).
971 53 Liberzon, A. *et al.* Molecular signatures database (MSigDB) 3.0. *Bioinformatics*
972 *(Oxford, England)* **27**, 1739-1740, doi:10.1093/bioinformatics/btr260 (2011).
973 54 Li, H. & Durbin, R. Fast and accurate long-read alignment with Burrows-
974 Wheeler transform. *Bioinformatics (Oxford, England)* **26**, 589-595,
975 doi:10.1093/bioinformatics/btp698 (2010).
976 55 Zhang, Y. *et al.* Model-based analysis of ChIP-Seq (MACS). *Genome biology* **9**,
977 R137, doi:10.1186/gb-2008-9-9-r137 (2008).
978 56 Quinlan, A. R. & Hall, I. M. BEDTools: a flexible suite of utilities for comparing
979 genomic features. *Bioinformatics (Oxford, England)* **26**, 841-842,
980 doi:10.1093/bioinformatics/btq033 (2010).
981 57 Shannon, P. *et al.* Cytoscape: a software environment for integrated models of
982 biomolecular interaction networks. *Genome research* **13**, 2498-2504,
983 doi:10.1101/gr.1239303 (2003).
984 58 Colaprico, A. *et al.* TCGAbiolinks: an R/Bioconductor package for integrative
985 analysis of TCGA data. *Nucleic acids research* **44**, e71,
986 doi:10.1093/nar/gkv1507 (2016).
987 59 Hanzelmann, S., Castelo, R. & Guinney, J. GSVA: gene set variation analysis for
988 microarray and RNA-seq data. *BMC Bioinformatics* **14**, 7, doi:10.1186/1471-
989 2105-14-7 (2013).
990 60 Abida, W. *et al.* Genomic correlates of clinical outcome in advanced prostate
991 cancer. *Proceedings of the National Academy of Sciences of the United States of*
992 *America* **116**, 11428-11436, doi:10.1073/pnas.1902651116 (2019).
993 61 Gu, Z., Gu, L., Eils, R., Schlesner, M. & Brors, B. circlize Implements and enhances
994 circular visualization in R. *Bioinformatics (Oxford, England)* **30**, 2811-2812,
995 doi:10.1093/bioinformatics/btu393 (2014).
996 62 Yokoyama, Y. *et al.* BET Inhibitors Suppress ALDH Activity by Targeting
997 ALDH1A1 Super-Enhancer in Ovarian Cancer. *Cancer Res* **76**, 6320-6330,
998 doi:10.1158/0008-5472.can-16-0854 (2016).
999 63 Yu, G., Wang, L. G. & He, Q. Y. ChIPseeker: an R/Bioconductor package for ChIP
1000 peak annotation, comparison and visualization. *Bioinformatics (Oxford,*
1001 *England)* **31**, 2382-2383, doi:10.1093/bioinformatics/btv145 (2015).
1002 64 Welch, R. P. *et al.* ChIP-Enrich: gene set enrichment testing for ChIP-seq data.
1003 *Nucleic acids research* **42**, e105, doi:10.1093/nar/gku463 (2014).

1004 65 Beltran, H. *et al.* Divergent clonal evolution of castration-resistant
1005 neuroendocrine prostate cancer. *Nature medicine* **22**, 298-305,
1006 doi:10.1038/nm.4045 (2016).
1007

Figure 1

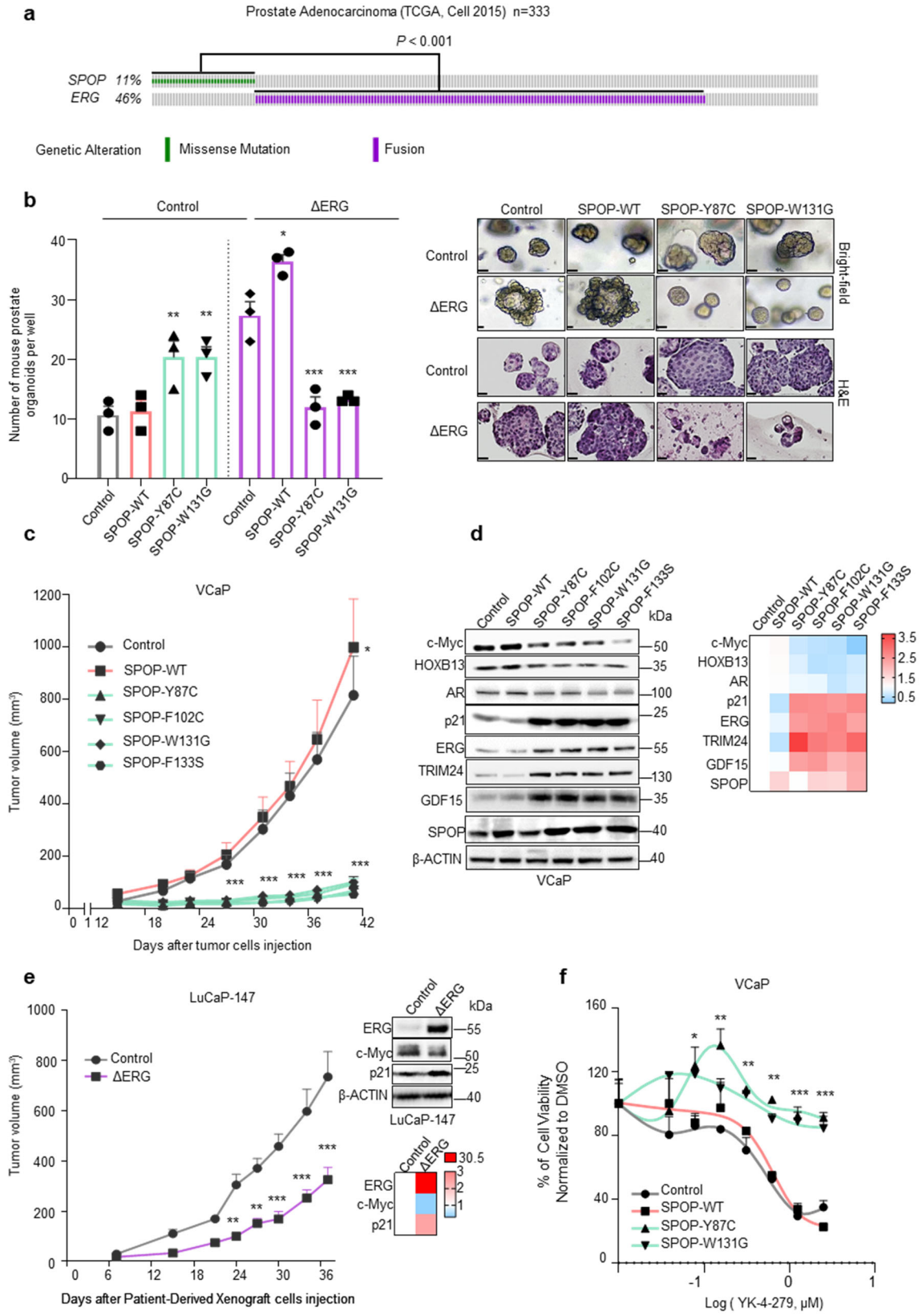
a
Prostate Adenocarcinoma (TCGA, Cell 2015) n=333
P < 0.001
SPOP 11%
ERG 46%
Genetic Alteration
Missense Mutation
Fusion
b
Control
ΔERG
Number of mouse prostate organoids per well
Control
SPOP-WT
SPOP-Y87C
SPOP-W131G
Bright-field
H&E
c
VCaP
Tumor volume (mm³)
Days after tumor cells injection
SPOP-F102C
SPOP-F133S
d
kDa
c-Myc
HOXB13
AR
p21
ERG
TRIM24
GDF15
SPOP
β-ACTIN
e
LuCaP-147
Days after Patient-Derived Xenograft cells injection
f
% of Cell Viability Normalized to DMSO
Log (YK-4-279, μM)

Figure 1. Genetic alterations in *SPOP* and *ERG* are synthetic sick. a, Distribution of genetic alterations in *SPOP* and *ERG* across 333 primary prostate cancers in TCGA database[1]. **b,** 3D growth of mouse prostate epithelial organoids derived from C57BL/6 mice over-expressing the indicated SPOP and ERG species (bar represents 20 μm) (n=3, technical replicates). Representative bright field pictures and haematoxylin and eosin (H&E) stained sections are shown. **c,** *In vivo* growth of VCaP xenografts over-expressing the indicated SPOP species in immune-compromised mice (each group, n=10). **d,** Immunoblot of VCaP cells over-expressing the indicated SPOP species and corresponding quantification of the indicated protein levels depicted as heatmap. Protein expression changes were normalized to β-ACTIN and Control cell line. **e**, Tumor growth kinetics of xenografts established from LuCaP-147 PDX (SPOP-Y83C) stably overexpressing ΔERG or Control vector (each group, n=10). Corresponding immunoblot and quantification depicted as heatmap. Protein expression changes were normalized to Vinculin (VCL) and Control cell line. **f,** Dose-response curve of VCaP cells overexpressing the indicated SPOP species and treated with the ETS-inhibitor YK-4-279. All error bars, mean + s.e.m. P values were determined by one-way ANOVA (b) or two-way ANOVA (c,e,f) with multiple comparisons and adjusted using Benjamini-Hochberg post-test $*P < 0.05$, $**P < 0.01$, $***P < 0.001$. Molecular weights are indicated in kilodaltons (kDa).

Figure 2

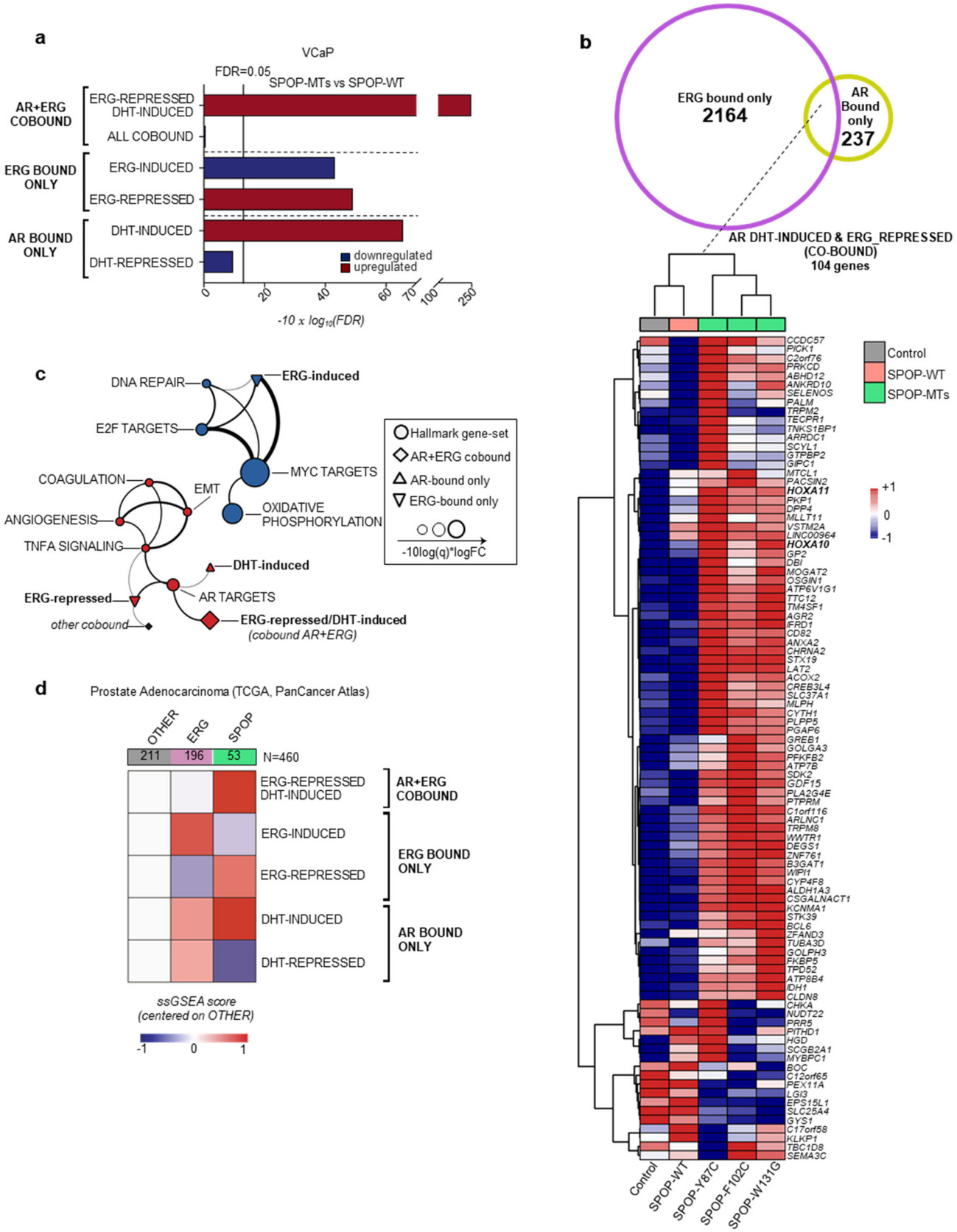
a
VCaP
FDR=0.05
SPOP-MTs vs SPOP-WT
AR+ERG COBOUND
ERG-REPRESSED DHT-INDUCED
ALL COBOUND
ERG BOUND ONLY
ERG-INDUCED
ERG-REPRESSED
AR BOUND ONLY
DHT-INDUCED
DHT-REPRESSED
downregulated
upregulated
0 20 40 60 70 100 250
-10 x log10(FDR)
b
ERG bound only
2164
AR Bound only
237
AR DHT-INDUCED & ERG_REPRESSED (CO-BOUND)
104 genes
Control
SPOP-WT
SPOP-MTs
+1
0
-1
Control
SPOP-WT
SPOP-Y87C
SPOP-F102C
SPOP-W131G
c
DNA REPAIR
ERG-induced
E2F TARGETS
MYC TARGETS
COAGULATION
EMT
ANGIOGENESIS
OXIDATIVE PHOSPHORYLATION
TNFA SIGNALING
DHT-induced
ERG-repressed
AR TARGETS
other cobound
ERG-repressed/DHT-induced
(cobound AR+ERG)
Hallmark gene-set
AR+ERG cobound
AR-bound only
ERG-bound only
-10log(q)*logFC
d
Prostate Adenocarcinoma (TCGA, PanCancer Atlas)
OTHER
ERG
SPOP
211
196
53
N=460
ERG-REPRESSED DHT-INDUCED
AR+ERG COBOUND
ERG-INDUCED
ERG-REPRESSED
ERG BOUND ONLY
DHT-INDUCED
DHT-REPRESSED
AR BOUND ONLY
ssGSEA score
(centered on OTHER)
-1
0
1

Figure 2. Mutant SPOP-induced androgen receptor signaling antagonizes ERG activity. a, Gene-set enrichment analysis of VCaP cells overexpressing SPOP mutant (SPOP-MTs; SPOP-Y87C, -F102C, -W131G) versus SPOP-wild type (-WT), based on RNA-seq data. Experiments were performed using three replicates for each condition. Enrichments are determined on custom gene-sets of direct androgen receptor (AR) and ERG target genes (Supplemental Table 1). Enrichments and FDR-adjusted p-values are computed with *Camera* (pre-ranked) **b,** Venn Diagram and heatmap depicting the expression of genes included in the custom gene-set of AR/ERG co-bound genes that are repressed by ERG and induced by DHT in VCaP cells overexpressing SPOP-MTs (SPOP-Y87C, F102C, W131G), SPOP-WT and vector Control. Genes (rows) and samples (columns) were clustered using Euclidean distance. Gene expression values, normalized using variance stabilizing transformation (vst) were scaled and centered by row prior of clustering. Columns represent average expression of three replicates for each condition. **c,** Two-dimensional network representing overlaps between the 10 most significantly enriched Hallmark and custom gene-sets, identified when comparing SPOP-MTs (SPOP-Y87C, F102C, W131G) to SPOP-wild type (-WT) overexpressing VCaP cells. Thickness of edges is proportional to the significance of the overlap of the connected nodes measured by Fisher test. Only edges with FDR value <0.05 are shown. Size of nodes is proportional to gene-set enrichment significance and equals to -10 x $\log_{10}$ (FDR). **d**, Heatmap representing gene-set activity stratified according to tumor subtype, derived from TCGA cohort. For each tumor group, the average value of single sample GSEA scores was considered. Values were scaled and referenced to samples that did not harbor any ETS-fusion (*ERG*, *ETV1*, and *ETV4)* or point mutations in *SPOP*[1].

Figure 3

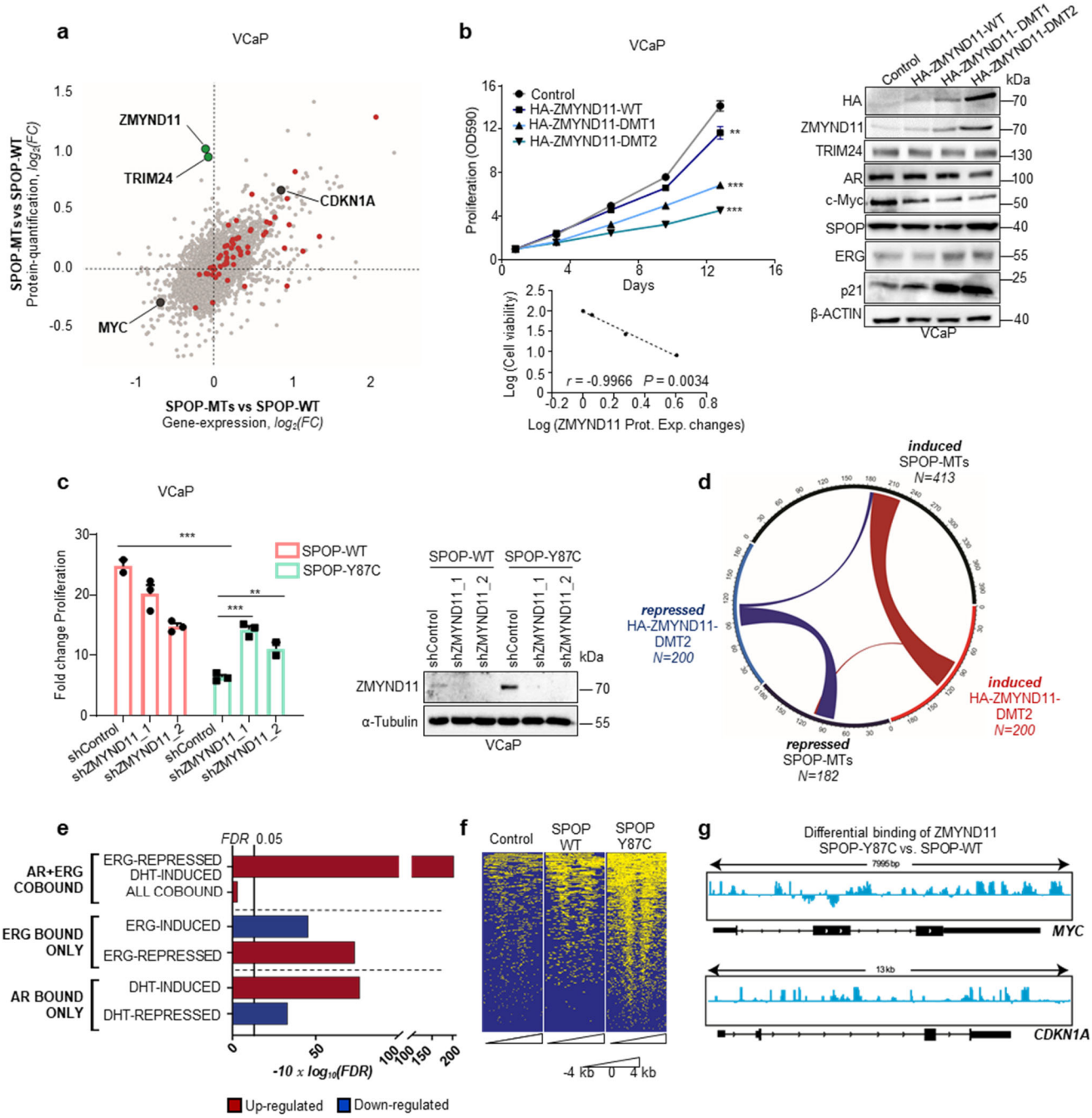

Figure 3. ZMYND11 is a SPOP substrate and influences AR- and ERG-dependent gene transcription. a, Scatter plot of SPOP-MTs (average across SPOP-Y87C, -F102C, -W131G) versus SPOP-WT transcriptome (n=3, biological replicates) and proteome expression changes in VCaP cells (n=2, biological replicates). Genes from custom signature DHT-Induced/ERG-Repressed genes (AR+ERG co-bound) are highlighted in red. TRIM24 and ZMYND11 are the most upregulated proteins without changes at mRNA levels and are highlighted in green. CDKN1A (p21) upregulated at both mRNA and protein

levels, and MYC downregulated at both mRNA and protein levels, are highlighted in black. **b,** 2D proliferation assay of VCaP cancer cells overexpressing HA-ZMNYD11-WT and derived degron-deficient mutants (DMT1/2) (n=3). Corresponding immunoblot of indicated proteins. Correlation between cell viability and ZMYND11 protein expression changes (Prot. Exp. Changes), as quantified by immunoblot in the same cell lines. *P* values were calculated using Pearson rank correlation. **c,** Fold-change cell viability of VCaP cancer cells over-expressing the indicated SPOP species with and without *ZMYND11* knockdown using two different short hairpin RNAs, at day 16 (n=3). Protein expression of the indicated proteins was analyzed by immunoblotting. **d,** Chord-diagram of transcriptionally regulated genes by either SPOP-MTs or HA-ZMYND11-DMT2 in VCaP cells (FDR<0.05). Strings, whose thickness is proportional to the number of shared elements, represent common genes between sets. **e,** Gene-set enrichment analysis of VCaP cell overexpressing HA-ZMYND11-DMT2 compared to Control, based on RNA-seq data. Enrichments are performed on custom gene-sets of direct androgen receptor (AR) and ERG target genes. FDR-adjusted p-values are computed with *Camera* (pre-ranked). **f**, Heatmap of ChIP-seq signals around TSS regions (+/- 4kb) at which ZMYND11 bindings were identified by peak calling procedure (Macs2). **g**, IGV-derived screenshots representing loglikelihood ratio of ZMYND11 bindings in mutant SPOP (SPOP-Y87C) vs wild-type SPOP over-expressing VCaP cells. Reported are *MYC* (up) and *CDKN1A* (bottom). All error bars, mean ± s.e.m. *P* values were determined by two-way ANOVA (**b**) or one-way ANOVA with multiple comparisons and adjusted using Benjamini-Hochberg post-test (**c**). $^{**}P < 0.01$, $^{***}P < 0.001$. Molecular weights are indicated in kilodaltons (kDa).

Figure 4

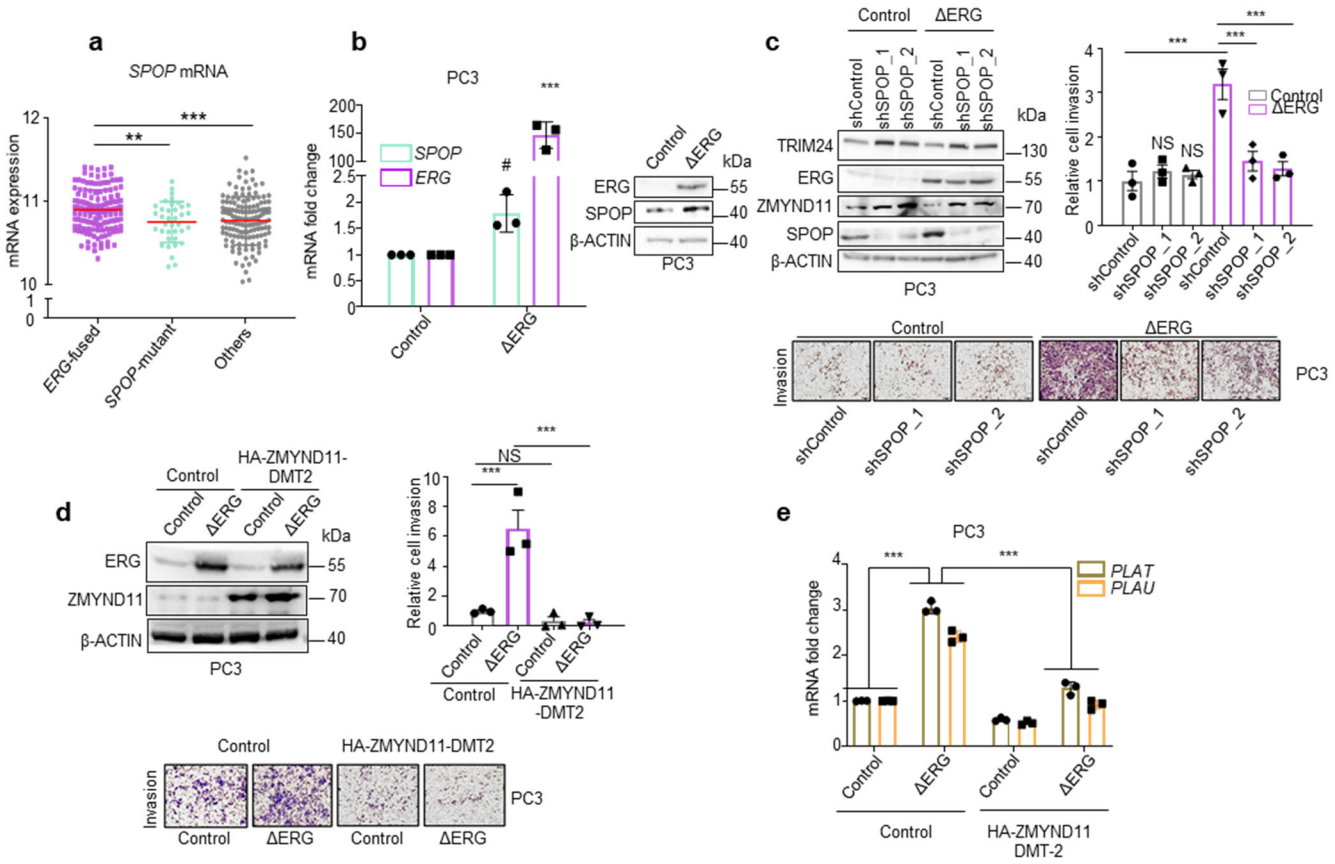

Figure 4. SPOP-WT is an ERG target gene and required for ERG-mediated cell invasion. a, *SPOP* mRNA expression levels in 333 primary prostate cancer tissues stratified according to the indicated driver mutations[1]. Error bars, mean ± s.d. **b,** SPOP mRNA and protein levels in response to forced expression of ΔERG in PC3 prostate cancer cells by qPCR and immunoblotting, respectively. Error bars, mean + s.e.m. (n=3). *P* values were determined by unpaired, two-tailed Student's t-test. $^{\#}P < 0.05$; Control versus ΔERG for *SPOP* expression levels. $^{***}P < 0.001$; Control versus ΔERG for *ERG* expression levels. **c,** Transwell Matrigel invasion assay of PC3 cells with forced expression of ΔERG and knockdown of SPOP using two different short hairpin RNAs. Protein expression of the indicated proteins was assessed in parallel by immunoblotting. Error bars, mean ± s.e.m. (n=3). **d,** Transwell Matrigel invasion assay of PC3 cells with forced expression of ΔERG and HA-ZMYND11-DMT2 and corresponding immunoblot analysis. Error bars, mean ± s.e.m. (n=3). **e,** Analysis of the ΔERG- and HA-ZMYND11-DMT2-induced transcriptional changes in the ERG target genes *PLAU* and *PLAT*. All error bars, mean ± s.e.m. *P* values were determined by one-way ANOVA with multiple comparisons and adjusted using Benjamini-Hochberg post-test (**a,c,d,e**). NS, not significant. $^{**}P < 0.01$, $^{***}P < 0.001$. Molecular weights are indicated in kilodaltons (kDa).

Figure 5

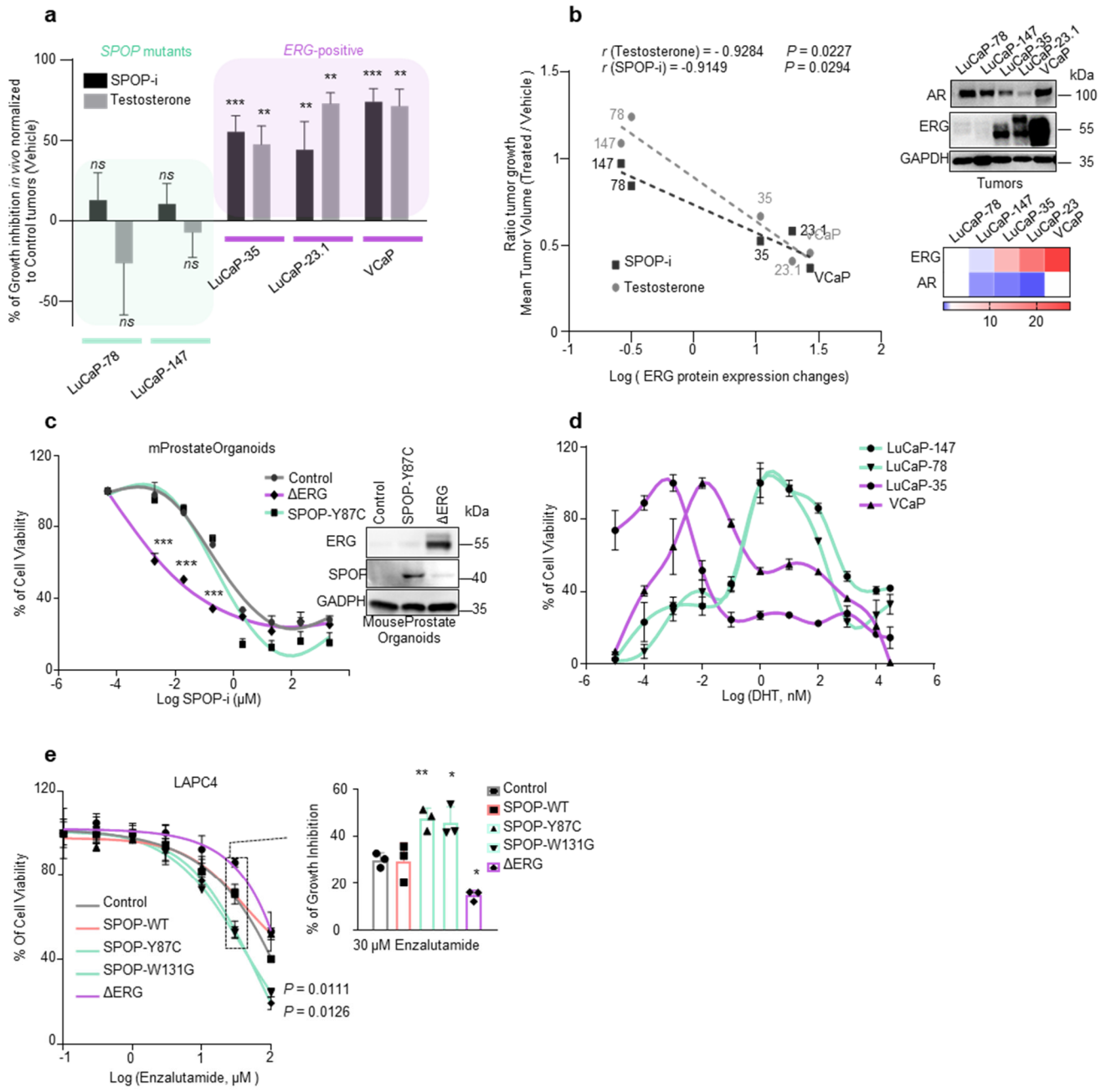

Figure 5. ERG and mutant SPOP trigger different responses to therapeutic interventions. a, Sensitivity to Testosterone and SPOP-i treatment in xenograft and PDX models. LuCaP-23.1, LuCaP-35 and VCaP are *ERG*-positive cancer cells. LuCaP-147 and LuCaP-78 are *SPOP* mutant cancer cells (respectively SPOP-Y83C and SPOP-W131G). Growth inhibition is calculated using the last tumor measurements as shown in Extended Data Fig. 8f-j and 9e-i. **b**, Correlation of sensitivity to SPOP-i or testosterone treatment shown in Extended Data Fig. 8f-j and 9e-i, with ERG protein levels, as quantified by immunoblot, in PDX models and xenografts. *P* values were calculated using Pearson rank correlation. Corresponding immunoblot and quantification of AR and ERG protein levels

depicted as a heatmap. Protein expression changes were normalized to GAPDH and LuCaP-78. **c,** Dose-response curves to SPOP-i treatment of Mouse Prostate Organoids overexpressing ΔERG, SPOP-Y87C and Control vector**. d,** Dose-response curves to DHT treatment of VCaP, LuCaP-35, LuCaP-78 and LuCaP-147 PDX cancer cells. Prior to DHT treatment, PDX were grown in standard media without DHT. VCaP were starved for 24h in CSS medium (RPMI + 10% charcoal-stripped serum). **e,** Enzalutamide sensitivity of LAPC4 cells overexpressing ΔERG or SPOP mutant species (Y87C, W131G). All error bars, mean + s.e.m. *P* values were determined by unpaired, two-tailed Student's t-test (**a**), $*P < 0.05$, $**P < 0.01$, $***P < 0.001$. Molecular weights are indicated in kilodaltons (kDa).

References

1 TCGA. The Molecular Taxonomy of Primary Prostate Cancer. *Cell* **163**, 1011-1025, doi:10.1016/j.cell.2015.10.025 (2015).